Powder Technology 429 (2023) 118939

Contents lists available at ScienceDirect

Powder Technology

journal homepage: www.journals.elsevier.com/powder-technology

A numerical sensitivity study – The effectiveness of RFID-based ore tracking through a simulated coarse ore stockpile and the impacts of key process variables

Juan Chen [a,*], Tien-Fu Lu [b], Dylan Peukert [a,c], Peter Dowd [a,c]

[a] ARC Training Centre for Integrated Operations for Complex Resources, The University of Adelaide, Adelaide, SA 5005, Australia
[b] School of Mechanical Engineering, University of Adelaide, South Australia 5005, Australia
[c] School of Civil, Environmental and Mining Engineering, The University of Adelaide, Adelaide, SA 5005, Australia

HIGHLIGHTS

- Proof of concept for three model fitting techniques applied to DEM data of a coarse ore stockpile.
- Model evaluates the effectiveness of RFID-based ore tracking technology.
- Sensitivity study is performed on the influence of several simulation variables.

GRAPHICAL ABSTRACT

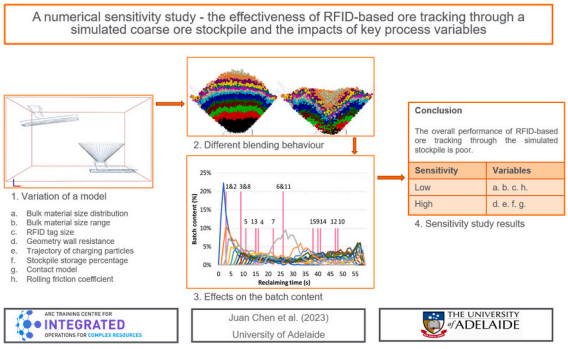

ARTICLE INFO

Keywords:
RFID tag
Ore tracking
Stockpile modelling
Discrete element method
Simulation

ABSTRACT

The ability to understand ore characteristics in real-time during mining processes is vital for ensuring product quality control. However, it is challenging to continuously track ore flow from the mine to the mill due to the blending of ore batches, especially within stockpiles. This paper presents a numerical study of copper ore tracking through a coarse ore stockpile. A discrete element model of a 3D stockpile was created using the EDEM software to evaluate the effectiveness of using RFID tags for ore tracking. To identify the primary variables and their effect on ore transport and tracking through the stockpile, a sensitivity study was conducted to investigate a range of process variables, such as ore size distribution, ore size range, RFID tag size, wall friction, the trajectory of charging particles and stockpile charging methods. The results show that the stockpile model is not sensitive to variables such as the ore size distribution, ore size range and RFID tag size, while wall friction, stockpile feed belt speed, segregation in the ore flow region and contact model have a significant effect on ore blending within the stockpile. It was found that the overall performance of RFID-based ore tracking through the stockpile is poor. For cases with only one or a few tags per ore batch the order in which the tags are read did not provide a good representation of the ore distribution for most scenarios This sensitivity study provides insights into new tracking strategies given the poor performance of RFID tracking shown by the simulation study.

* Corresponding author.
E-mail address: juan.chen@adelaide.edu.au (J. Chen).

https://doi.org/10.1016/j.powtec.2023.118939
Received 9 March 2023; Received in revised form 16 August 2023; Accepted 23 August 2023
Available online 24 August 2023

1. Introduction

Copper recovery and energy consumption in mineral processing depend on the characteristics of the ore sent for processing from upstream operations. Successful extraction of mineral resources requires a thorough understanding of the spatial distribution of ore grades and tonnages throughout the mining process. The quality of the produced copper ore concentrate needs to be controlled in order to meet the requirements for sale. Therefore, it is vital to know the characteristics of ore being fed to the mill to control the operations in order to maximise economic benefit. Radio frequency identification (RFID) is one of the foundational technologies for tracking and integrating data sets in mining processes. RFID technology has been primarily employed in the mining sector for applications such as tracking the location of vehicles and miners' [1,2], access control, and safety management [3]. The concept of using RFID tags to track ore was first tested in 2007 at Vale Inco's copper-nickel Frood-Stobie mine [4]. The experiment allowed the output of the mine to be estimated enabling the preparation of the necessary chemicals for processing the copper and nickel ore. RFID methodologies also provide the possibility of tracking granular material flows [5] and have the potential to link processed ore batches back to their underground source in real time [6]. For tracking bulk material, RFID tags can be used to mark the beginning and end of a copper ore batch. The accuracy of the ore tracking will depend on how representative the distribution of read RFID tags is of the ore flow. The general concept of RFID-based ore tracking includes the following procedures: analyse input ore characteristics, associate the information with the RFID tags, add the tags to the transported ore, transport ore together with the tags, read the information from the tags and use it to facilitate control of ore processing in the processing plant [7].

There are challenges to developing ore-tracking methods, resulting from the thorough blending of non-homogenous, bulk raw material flows in the dynamic context of a mine. The characteristics of the copper ore can be identified at mining faces, but blending may occur in various subsequent stages, such as blasting, transportation, conveying, stockpiling, and reclaiming. Although this blending can smooth out differences in production qualities between ore sources, it increases the difficulty of providing accurate information of the processed ore in real-time. There are several methods for real-time tracking and monitoring the quantity and quality of excavated material during transportation, such as advanced imaging technologies, computer vision techniques, and RFID-based tracking systems. Advanced imaging technologies such as 3D laser scanners or structured light scanners can help determine ore quality by providing detailed information on ore characteristics, such as size distribution, shape and mineral composition [8]. Computer vision techniques can be employed to analyse images or videos of the excavated material, enabling automated tracking and identification. Passive RFID tags have been used to track iron ore transportation [9]. RFID tags have also been used to investigate ore flows through process hold-ups such as bins, bunkers and stockpiles for metal accounting and process control [10,11]. RFID tag tracking can contribute to estimating the residence time for different ore batches that are delivered to coarse ore stockpiles (COS) and assist in monitoring the blending of ore batches in real time within the COS [12]. One of the key challenges for developing a reliable tracking system is the segregation and stratification of coarse and fine particles, which is common during material transport through process hold-ups [13]. As the stockpile is typically the last step in the ore transport system prior to milling, the quality of blended ore can directly affect the mill's performance. For most mining operations, the segregation and stratification of fine and coarse particles can also complicate the tracking of the RFID tags as the tags used are smaller than most particles [14,15]. However, for some cases, such as for iron ore pallet feed blending operations, this issue is not present due to differing particle sizes. The passive RFID technique has been previously tested to investigate potential improvements in traceability throughout the distribution chain [16,17]. In these studies, the authors investigated various shapes and sizes, and it was found that larger RFID tags were not significantly segregated from the iron ore pellets [18]. In cases where such segregation does occur, the RFID tag may not represent the ore batch it was originally associated with. Hence, it is vital to understand the blending behaviour of the COS, to enable reliable tracking of ore production. In addition, better knowledge of blending behaviour and residence time of ore batches and RFID tags through COSs are beneficial to process improvement and product quality control.

Over the last few decades, the discrete element method (DEM) has emerged as one of the most versatile numerical modelling methods and has been widely used to model granular dynamics and to simulate equipment handling of mined material. The DEM method, developed by Cundall and Strack in 1979 [19,20], models particle-particle and particle-surface interactions as well as other dynamic behaviours over time. The DEM method has been extensively applied to analyse bulk material flows in mining equipment, including bunker charging and discharging [11,21], conveyor transfer [22], semi-autogenous grinding (SAG) mills [23], jaw crushers [24], and transfer chutes [25]. Dolman [26] used DEM to model material flow and size distribution of ore in a stockpile. Gomez et al. [27] found it was possible to use DEM to represent the natural segregation process of stockpiles of rock materials. Yu et al. [13] validated DEM as a viable option for investigating the process of stockpile formation. Zhang et al. [28] conducted a numerical study based on DEM to explore stockpile segregation.

The reviewed literature reveals that research on the ore flow through COSs has been limited, and that the effectiveness of RFID-based ore tracking through COSs has not been investigated. Most of the reviewed DEM simulations consider laboratory-scale models, with a relatively low number of particles. Additionally, most stockpile models have limited utility for quality control applications as it is difficult to model the stockpile accurately so as to be as close as possible to reality [29]. The challenge of modelling COSs is the high number of particles, up to millions or even billions of particles. Usually the size of the stockpile model is scaled down or the 3D model is replaced by slices in order to reduce the computational time [26]. However, the material flow through a slice will be very different to a 3D COS due to the change in geometry. Hence, a full understanding of the dynamic blending behaviour of the 3D COS could not only contribute to developing an effective ore tracking model, but also to improve the productivity and profitability of mineral processing.

This paper presents a systematic sensitivity analysis of ore and tag blending behaviour applied to selected uncertain EDEM variables, such as particle size distribution and range, RFID tag size, wall friction, conveyor belt speed, stockpile charging and discharging methods, and the contact model used to generate the simulation predictions. The sensitivity analysis can quantify the impact of each input variable on the model output, enabling identification of the dominant variables for future applications. The results of the sensitivity study can assist in providing a better understanding of how RFID tag ore tracking performs during stockpile discharging and apron feeder reclaiming procedures. This information may lead to a better understanding of how to implement proper ore tracking procedures based on the site material properties and equipment conditions.

The structure of this paper is as follows. Section 2 illustrates the methodology and variables used to simulate the COS system, followed by a sensitivity study of the DEM variables. Section 3 introduces the results of the simulation, including both qualitative images and quantitative data obtained from the EDEM software. Discussion is provided to accompany the results where necessary in Section 4. Section 5 draws some conclusions from this study.

2. Methodology

2.1. The discrete element method (DEM)

In the DEM, individual granular particles and the interactions between spherical particles are modelled. The position and orientation of a new particle in a granular system can be calculated by numerical integration of the following equations, derived from Newton's second law of motion [30]:

$$m_i\frac{du_i}{dt}=\sum_{j=1}^{N}\left(F_{ij}^{cn}+F_{ij}^{ct}+F_{ij}^{dn}+F_{ij}^{dt}\right)+F_i^g \tag{1}$$

$$I_i\frac{d\omega_i}{dt}=\sum_{j=1}^{N}\left(M_{ij}\right) \tag{2}$$

where m_i and I_i are the mass and inertia of particle i and $v_i$and ω_i are the translational and angular velocity of particle i. The modelled forces include contact forces (F_{ij}^{cn},F_{ij}^{ct}), damping forces (F_{ij}^{dn},F_{ij}^{dt}) and the gravitational force F_i^g. The contact forces and damping forces are the sum of the forces in the normal and tangential directions. M_{ij} is the sum of torques acting on the particle.

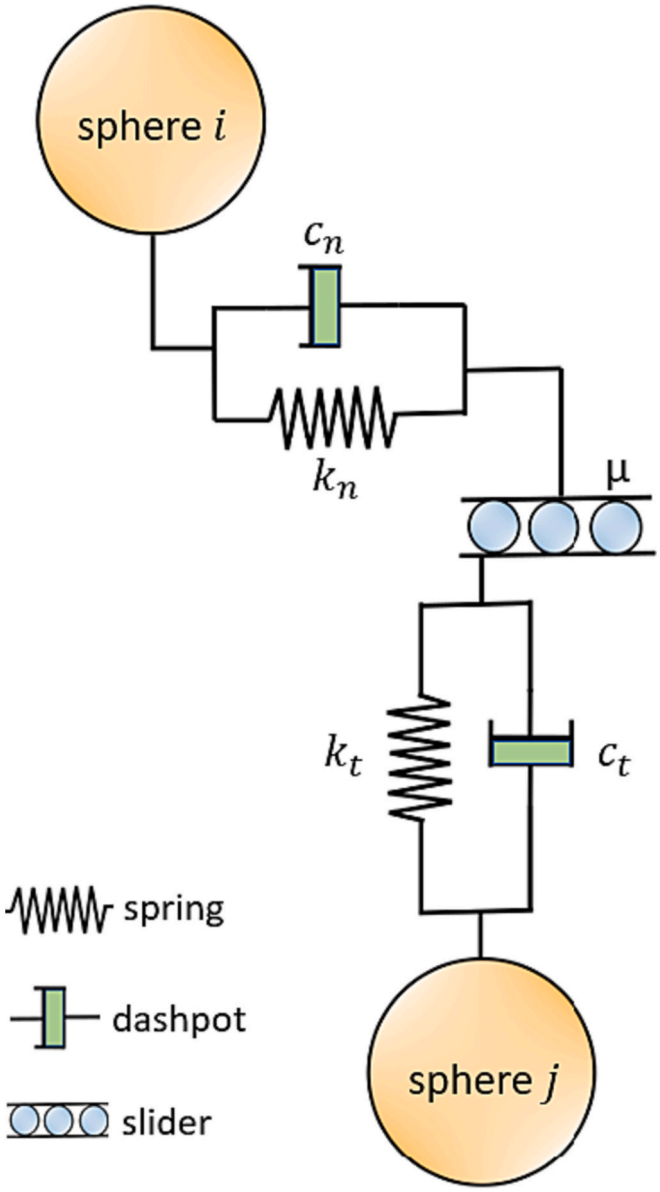

Fig. 1. Contact model of particles in the EDEM.

Fig. 1 illustrates the contact model used in the DEM, using a spring and a dashpot to represent the elastic and plastic nature of particles in the normal direction. In the tangential direction, the model consists of a slider, a spring, and a dashpot.

The normal contact force F_{ij}^{cn} and normal damping forces F_{ij}^{dn} are given by (3) and (4) [31–33]:

$$F_{ij}^{cn}=\frac{4}{3}E_{eqv}\sqrt{R_{eqv}}\delta_n^{\frac{3}{2}}n_{ij} \tag{3}$$

$$\frac{1}{E_{eqv}}=\frac{\left(1-v_i^2\right)}{E_i}+\frac{\left(1-v_j^2\right)}{E_j} \tag{3a}$$

$$n_{ij}=\frac{x_i-x_j}{|x_i-x_j|} \tag{3b}$$

$$R_{eqv}=\frac{R_iR_j}{R_i+R_j} \tag{3c}$$

$$F_{ij}^{dn}=-2\sqrt{\frac{5}{6}}\frac{lne}{\sqrt{ln^2e+\pi^2}}\sqrt{k_nm_{eqv}}v_{ij}^n \tag{4}$$

$$k_n=2E_{eqv}\sqrt{R_{eqv}\delta_n} \tag{4a}$$

where E_{eqv}, m_{eqv} and R_{eqv} are the equivalent Young's modulus, mass and radius of the DEM sphere [34,35], δ_n is the overlap in the normal direction, n_{ij} is unit vector, v is the Poisson ratio, e is the coefficient of restitution, v_{ij}^n is the normal component of the relative velocity and k_n is the normal stiffness.

The tangential contact force F_{ij}^{ct} and the tangential damping force F_{ij}^{dt} are given by (5) and (6):

$$F_{ij}^{ct}=-k_t\delta_t \tag{5}$$

$$k_t=8G_{eqv}\sqrt{R_{eqv}\delta_n} \tag{5a}$$

$$G_{eqv}=\sqrt{\frac{G_iG_j}{G_i+G_j}} \tag{5b}$$

$$F_{ij}^{dt}=-2\sqrt{\frac{5}{6}}\frac{lne}{\sqrt{ln^2e+\pi^2}}\sqrt{k_tm_{eqv}}v_{ij}^t \tag{6}$$

where k_t is the tangential stiffness, δ_n is the tangential overlap vector, G_{eqv} is the equivalent shear modulus and, v_{ij}^t is the relative tangential velocity.

A rolling friction must be included in order to properly model the rotational motion of particles and account for non-spherical properties of materials that are difficult to simulate such as sharp edges and edge roundness. The tangential forces are limited by a Coulomb friction model (7) and the rolling friction. The applied torque depends on the normal force, particle radius and angular velocity (8):

$$F_{ij}^{ct}+F_{ij}^{dt}\le\mu_sF_{ij}^{cn} \tag{7}$$

$$\tau_i=-\mu_rF_{ij}^{cn}R_i\omega_i \tag{8}$$

where μ_r is the coefficient of rolling friction, R_i is the distance of the contact point from the centre of mass, and the ω_i is the unit angular velocity vector [36].

During the simulation process, the interactions of particles are driven by the forces and torques defined in Eqs. (3–8).

While DEM has proven to be a valuable tool for understanding the

dynamics of granular systems, it has certain limitations in modelling the transport of crushed ore, especially for modelling of the coefficient of friction on the contact of different materials. DEM simulations require input parameters, such as particle properties, contact properties, and friction coefficients, to be specified. The values of these physical parameters of materials and physical models of particle interaction can have a significant impact on the simulation results [37]. However, determining the appropriate friction coefficients for different material combinations is often challenging, as they can vary depending on factors such as moisture content, particle size distribution, and surface conditions. In DEM, friction between particles is typically modelled using simplified contact models, such as the linear-spring-slider or linear-spring-dashpot models. These models assume a constant coefficient of friction between particles, irrespective of the material properties or surface roughness. However, the coefficient of friction can vary significantly between different materials and surfaces, leading to limitations in accurately representing the true friction for all the interactions of the transported ore particles. Additionally, the constant coefficient of friction in DEM often primarily represents the static friction between particles in contact. However, in dynamic situations, such as during the

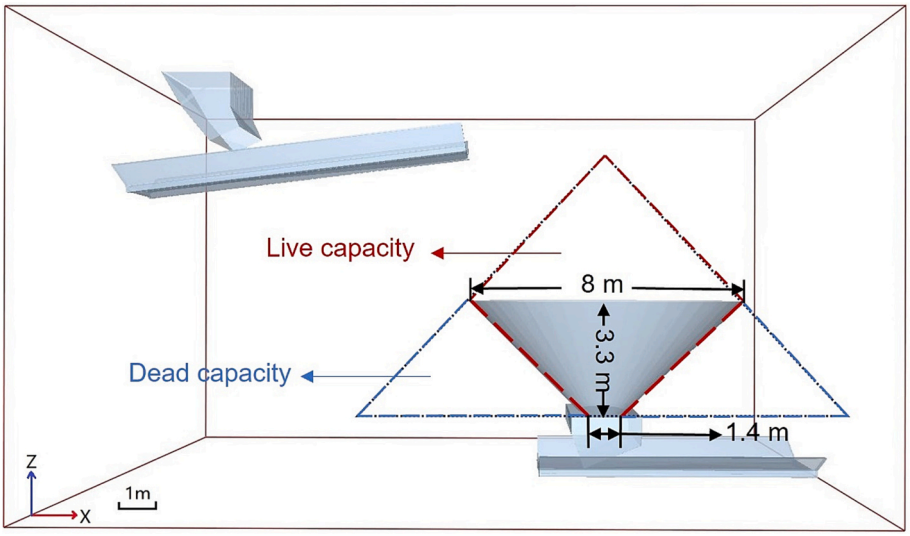

Fig. 2. 3D geometry model of the COS system in EDEM.

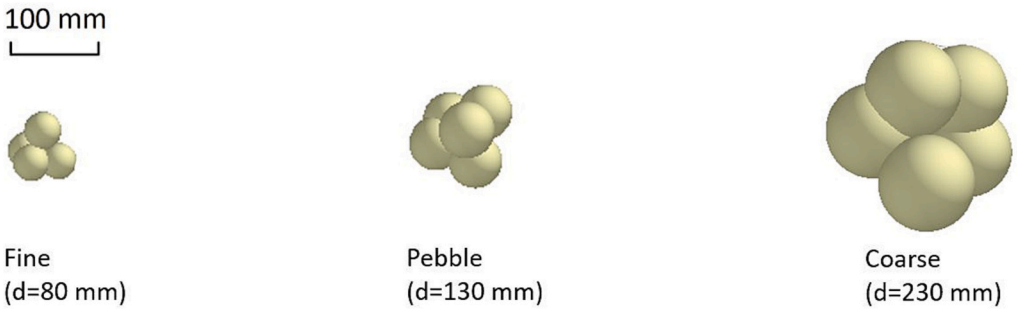

Fig. 3. Approximate modelling of real ore particles.

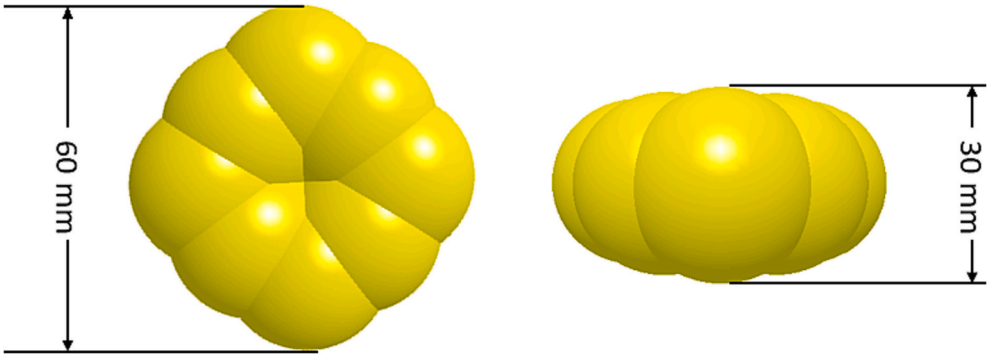

Fig. 4. Showing realistic irregularity of RFID tag.

Table 1
Design variables for the COS system.

Design variables	Value
Stockpile (live capacity) bottom radius (mm)	700
Stockpile (live capacity) top radius (mm)	4000
Stockpile (live capacity) length (mm)	3300
Stockpile wall withdrawal angle (degree)	45
Feed conveyor speed (mm/s)	4000
Feed conveyor belt length (mm)	10,000
Feed conveyor belt width (mm)	1000
Conveyor feed belt inclination angle (degree)	7
Apron feeder belt length (mm)	8000
Apron feeder belt width (mm)	1200
Apron feeder belt speed (mm/s)	1000

Table 2
Value of material properties*.

Property	Symbol	Value
Particle (fine) Diameter (mm)	D_f	80
Particle (pebble) Diameter (mm)	D_p	130
Particle (coarse) Diameter (mm)	D_c	230
Particle density — ore (kg/m^3)	ρ_o	2750
Particle density — tag (kg/m^3)	ρ_t	925
Solid density — wall (kg/m^3)	ρ_w	2750
Solid density — steel (kg/m^3)	ρ_s	7800
Solid density — conveyor belt	ρ_b	950
Young's modulus — ore (N/m^2)	E_o	1.25e+8
Young's modulus — tag (N/m^2)	E_t	1e+8
Young's modulus — wall (N/m^2)	E_w	1.25e+8
Young's modulus — steel (N/m^2)	E_s	1e+11
Young's modulus — belt (N/m^2)	E_b	5e+7
Poisson's ratio — ore	υ_o	0.25
Poisson's ratio — tag	υ_t	0.38
Poisson's ratio — wall	υ_w	0.25
Poisson's ratio — steel	υ_s	0.3
Poisson's ratio — belt	υ_b	0.45

Table 3
Interactions between ore and other simulated materials.

	ore - ore	ore - tag	ore - belt	ore - steel	tag - belt	tag -steel
Coefficient of Restitution*	0.3	0.2	0.2	0.1	0.4	0.1
Coefficient of Static Friction*	0.25	0.2	0.2	0.3	0.7	0.3
Coefficient of Rolling Friction	0.1*	0.01	0.01	0.01	0.2*	0.01

* Estimated value from the literature [11,26,39].

Table 4
Variables investigated in the sensitivity study.

Categories	EDEM variables	Baseline scenario (S1): value	Scenario: values
Bulk material size distribution	ore size distribution (pebble percentages)	S1: 80% (fine 10%; coarse10%)	S2: 70% (fine 15%; coarse15%) S3: 60% (fine 20%; coarse20%)
	ore size distribution (fine percentages)	S1: 10% (pebble 80%)	S4: 5% (pebble 80%) S5: 15% (pebble 80%) S6: 10% (pebble 70%) S7: 20% (pebble 70%) S8: 25% (pebble 60%) S9: 30% (pebble 60%)
Bulk material size range	ore size range (mm)	S1: 80 mm – 230 mm	S10: 40 mm – 270 mm S11: 50 mm – 260 mm S12: 60 mm – 250 mm S13: 70 mm – 240 mm
RFID tag size	RFID tag size (mm)	S1: d = 60 mm	S14: 70 S15: 80 S16: 90 S17: 100
Wall resistance	coefficient of static friction	S1: fs = 0.25	S18: fs = 0.5 S19: fs = 0.75 S20: fs = 1
Trajectory of charging particles	stockpile feed belt speed (m/s)	S1: CVD = 4 m/s	S21: CVD = 2 m/s S22: CVD = 3 m/s S23: CVD = 5 m/s
Stockpile storage percentage	stockpile storage percentage	S1: 100%	S24: 80% S25: 70% S26: 60%
Contact model	Contact model	S1: Hertz-Mindlin no slip (default) contact model	S27: linear spring-dashpot (LSD) contact model; characteristic velocity: 5 m/s S28: Hertz-Mindlin with JKR JKR-10 J-0.3SF-0.06RF
Coefficient of rolling friction	Coefficient of rolling friction between ore and tag	S1: 0.01	S29: 0.03 S30: 0.06 S31: 0.1
	Coefficient of rolling friction between ore and belt	S1: 0.01	S32: 0.03 S33: 0.06 S34: 0.1

transport of crushed ore on conveyor belts, the coefficient of friction can change due to factors such as particle velocity, vibration, and surface roughness. Neglecting these dynamic changes in friction can result in inaccurate predictions of material flow and behaviour.

2.2. The coarse ore stockpile model

A 3D model of the geometry of a COS system, which includes a hopper, a stockpile feed conveyor, a COS, one apron feeder and a virtual RFID reader was created using Autodesk Inventor Professional 2021 as shown in Fig. 2. The geometry was integrated into a DEM model and the system was simulated with Altair EDEM 2021.1 primarily using the default Hertz–Mindlin no slip contact model [38]. The geometry of the COS system was simplified in the model to facilitate computational efficiency and ease of analysis. The 3D conical stockpile shown in Fig. 2 was used to represent the stockpile live zone while the dead zone was approximated as the wall of the conical stockpile. The stockpile was assumed to have a wall angle of 45°. While the model uses a smooth and flat plate for the conical section, the properties were chosen to represent ore particles following the technique used by Dolman [26]. The ore discharging rate was set to approximately 4680 t per hour (tph), representing the realistic conditions of a mine. While some simplifications have been made for computational efficiency, the model was designed to accurately simulate the fundamental behaviour and dynamics of the COS system. It is worth noting that future studies could explore more detailed and accurate representations of the COS system by incorporating additional components and finer-scale geometry. However, for the objectives of this research and given current computational limitations, the simplified model serves as a valuable tool for analysing the

Fig. 5. Variables investigated in the sensitivity study (a) bulk material size distribution, (b) bulk material size range, (c) RFID tag size, (d) stockpile wall resistance, (e) trajectory of charging particles, (f) stockpile storage percentage, (g) coefficient of rolling friction.

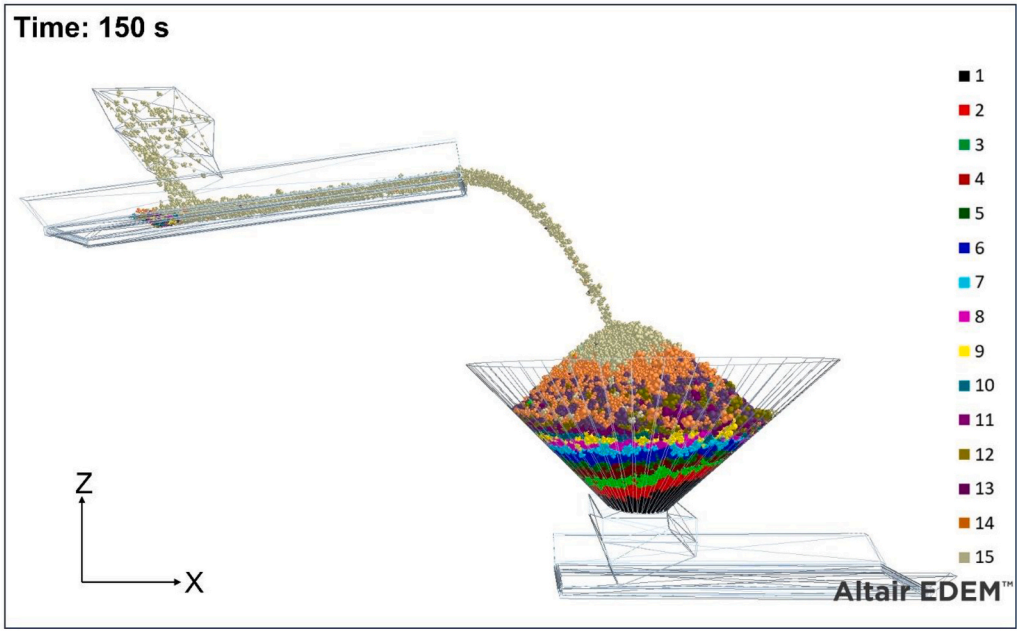

(a) t = 150 s

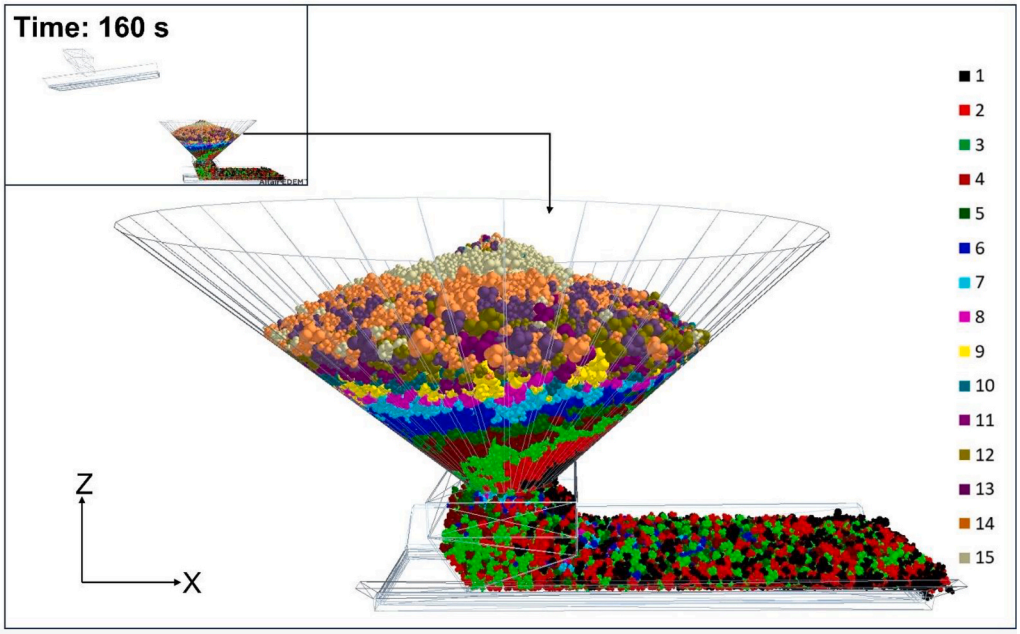

(b) t = 160 s

Fig. 6. Ore flow during the apron feeder reclaiming process in the EDEM software at (a)150 s, (b) 160 s, (c) 190 s, (d) 210 s.

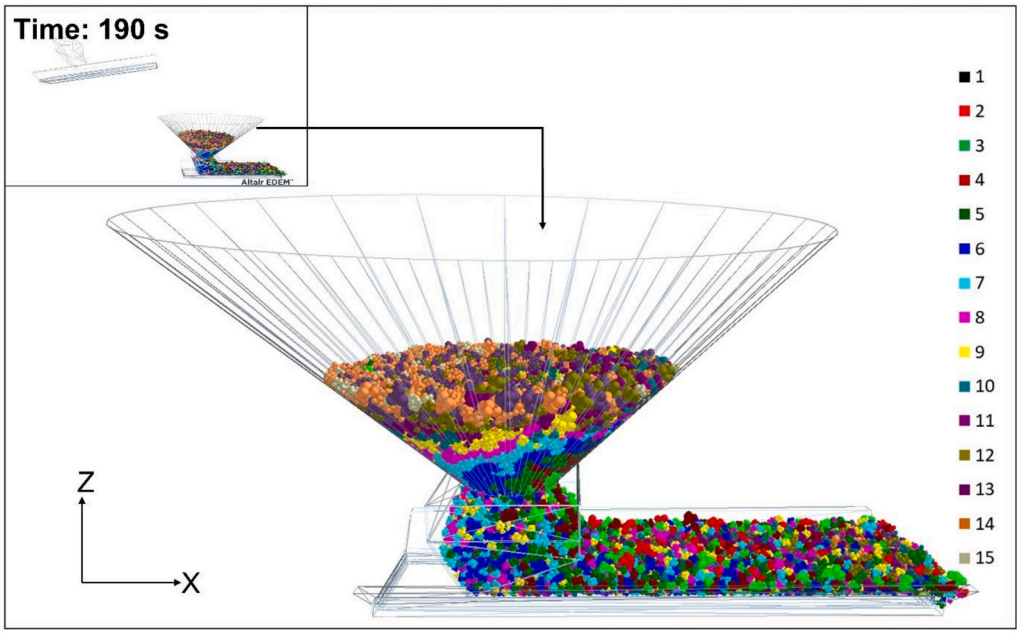

(c) t = 190 s

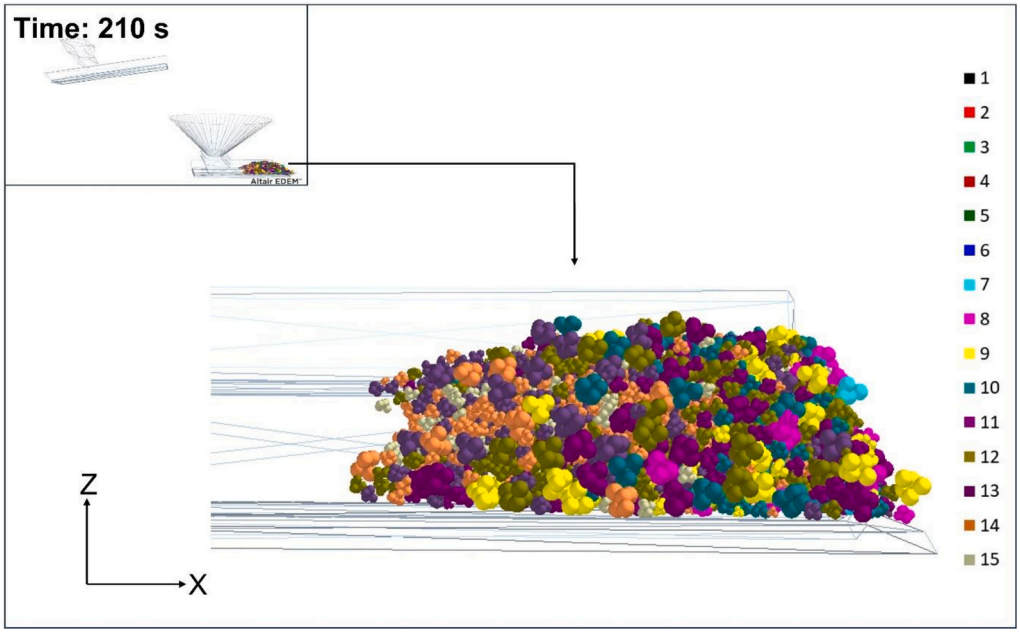

(d) t = 210 s

Fig. 6. (*continued*).

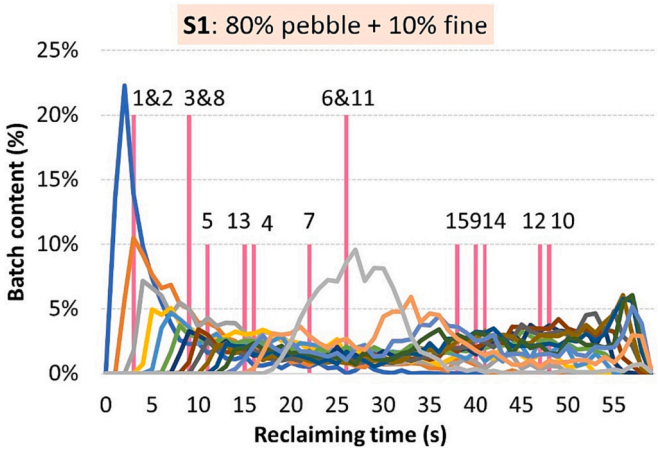

Fig. 7. EDEM simulation result of basic scenario (10% fine+80% pebble+10% coarse).

performance of using RFID tags to track ore through the COS system under various operational scenarios.

For a large number of particles of different types, the default model has the best performance. The default model simulates the particles as non-cohesive dry material and bonds were not required. Often for large-scale DEM simulations, variables are scaled to reduce the computational time [39]. To maintain proper bulk material behaviour, the particle size has not be increased for this study; instead, the size of the modelled stockpile is reduced in order to ensure a reasonable computational time. The Phoenix supercomputer at the University of Adelaide has a Lenovo NeXtScale system consisting of 260 nodes over 900 CPU and GPUs. It takes approximately 30 h for one simulation using 64 cores of the Phoenix HPC. The simulation represents a typical industrial coarse ore stockpile at a scale of approximately 1:6.

Copper ore is fed to the COS via a feed conveyor with a capacity of approximately 500 kg/s. The approximately 45,000 simulated particles are separated into 15 equal ore batches, each represented by a different colour. The ore batches are continuously and serially fed into the feed conveyor belt in order from 1 to 15 with each batch being fed over an interval of 10 s. In this study, a simplified size distribution, consisting of three particle sizes representing fine, pebble and coarse particles was modelled. For the baseline scenario (Scenario 1), each modelled ore batch contains 5 t of ore which is composed of 10% fines, 80% pebbles and 10% coarse particles, with diameters of 80, 130 and 230 mm respectively (Fig. 3). RFID tags are placed at the beginning of each ore batch to demarcate the change in ore batches. The clump representations of the RFID tag particle shape used in the current study can be seen in Fig. 4. The elongated particles were represented by 8 equal-sized spheres clumped together. The RFID tags are modelled to be representative of the Metso smart tag with a diameter of 60 mm and a thickness of 30 mm [40]. The stockpile charging process (0–150 s) and apron feeder reclaiming process (150–213 s) are modelled in the simulation. Table 1 lists the COS system variables for the baseline scenario. The discharge of ore from a cylinder through an open gate in the base of the cylinder matching the gate in the stockpile model was simulated to determine the wall angle. The wall angle was measured from the repose angle of the remaining ore within the cylinder and was found to be approximately 45°, which is consistent with the withdrawal angle measured by Dolman [26].

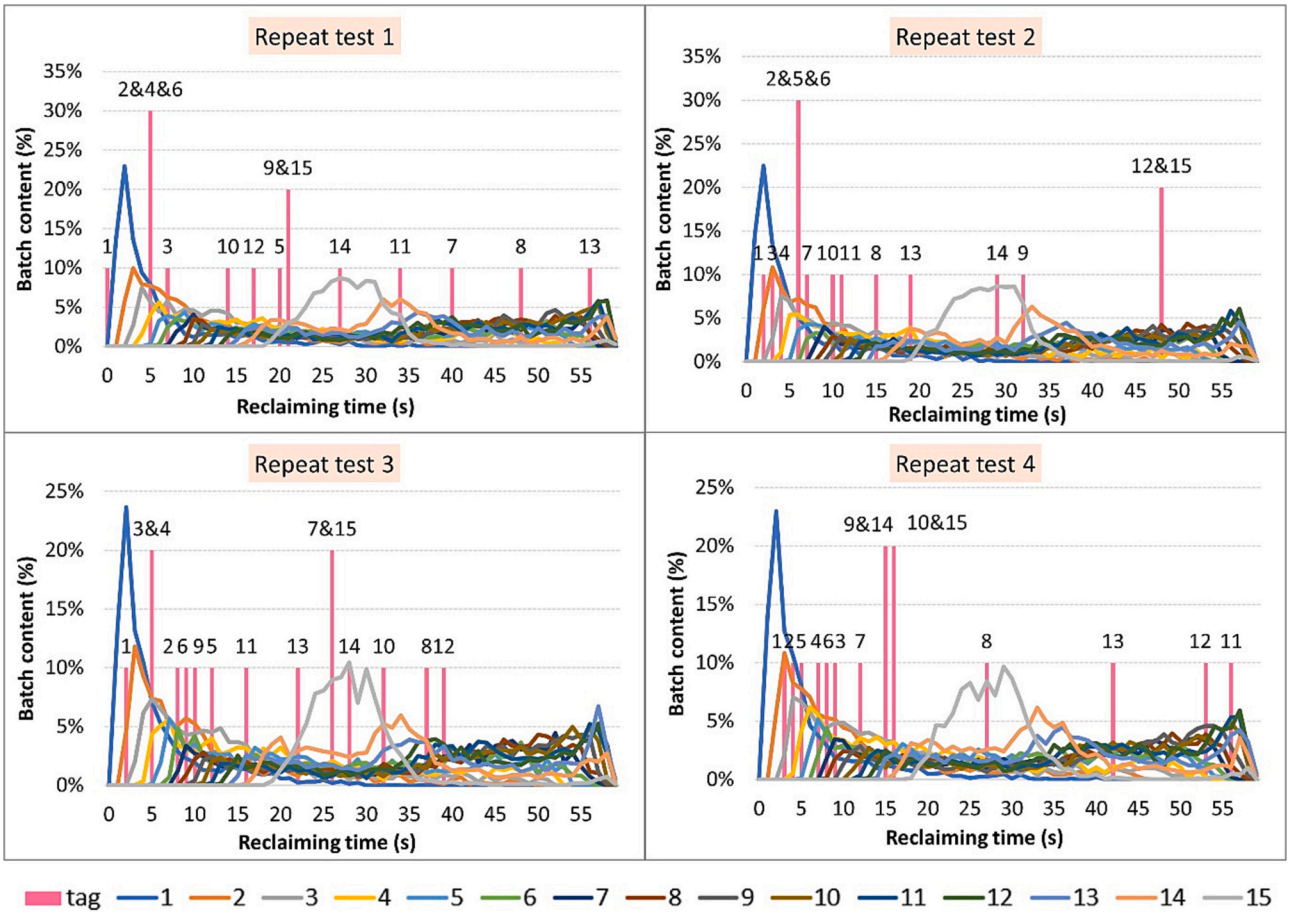

Fig. 8. Repeat test results for baseline scenario.

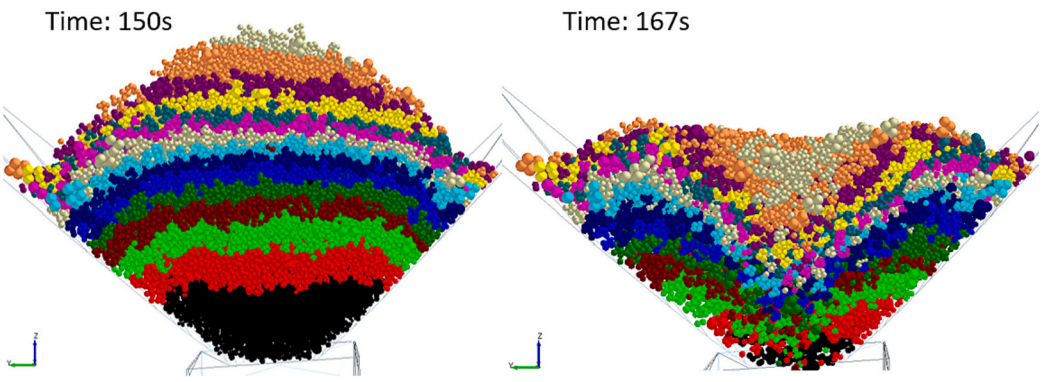

Fig. 9. EDEM simulation slice showing ore flow at $t = 150$ s and $t = 167$ s.

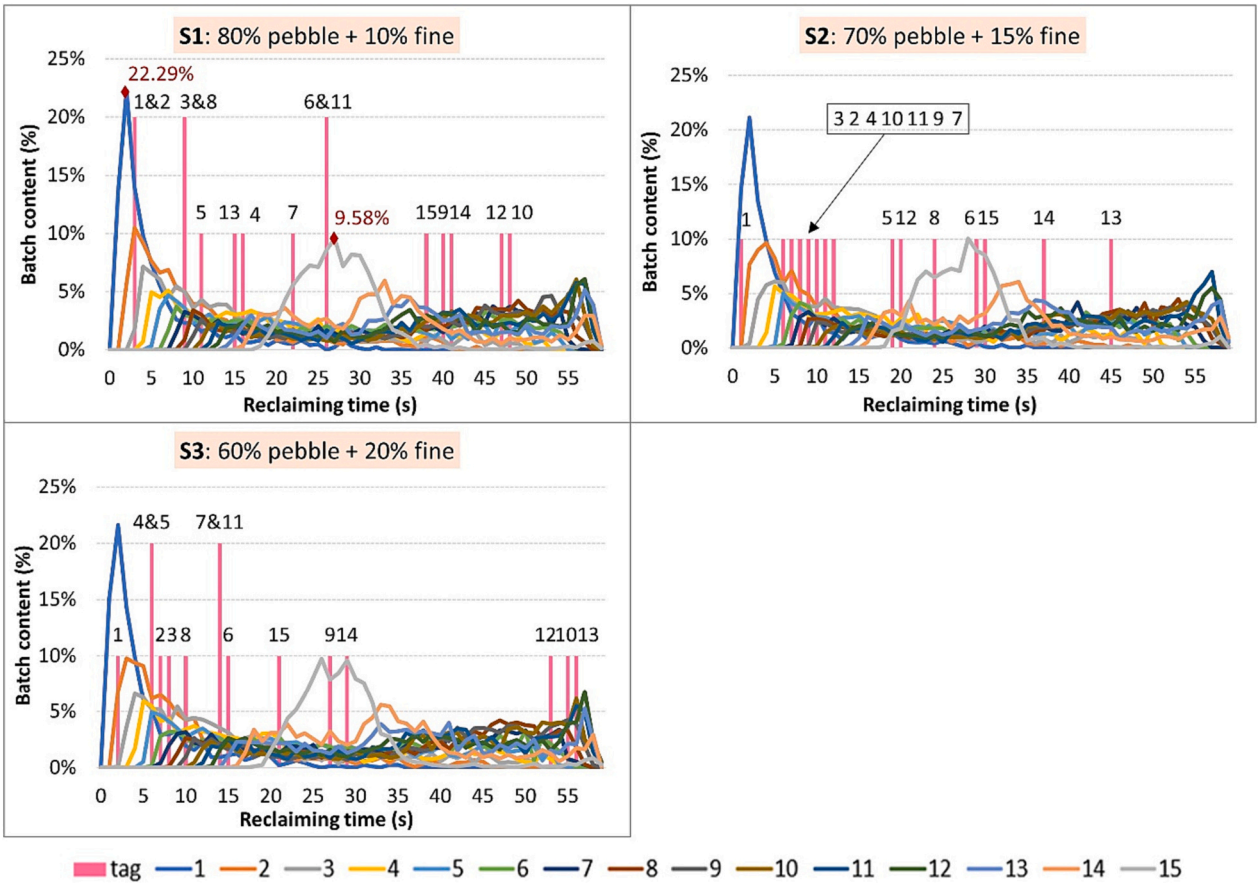

Fig. 10. Sensitivity analysis of ore tracking through COS with respect to ore size distribution (Scenarios 1 to 3).

2.3. COS model parameters and calibration

The properties of the copper ore particles, tags and other components of the modelled baseline COS system are listed in Table 2. Our work is based on Dolman's [26] study described above, using the same material properties and parameter values except for the coefficient of rolling friction between ores, tags and steel. In the DEM model, bulk density is required to accurately model the bulk material behaviour. The bulk density is determined by particle density and the packing efficiency of the particles. A particle density of 2750 kg$\hat{}$m^{-3} was chosen to be representative of a typical copper ore. The bulk density was assumed to be 60% of the particle density based upon the study by Schulze [41] and is therefore 1640 kg$\hat{}$m^{-3}. Irregularly shaped particles result in the formation of larger open voids within the volume, leading to a decrease in the overall bulk density. A higher bulk density indicates a greater degree of particle compaction and reduced void space, which can influence the material flow and the resistance to movement. Conversely, material with lower bulk density have a higher propensity for segregation during transportation.

An angle of repose test for qualitative calibration was performed in this study to calibrate the particle shape and sizes. According to Dolman's research, clusters of four or more spheres achieved a good

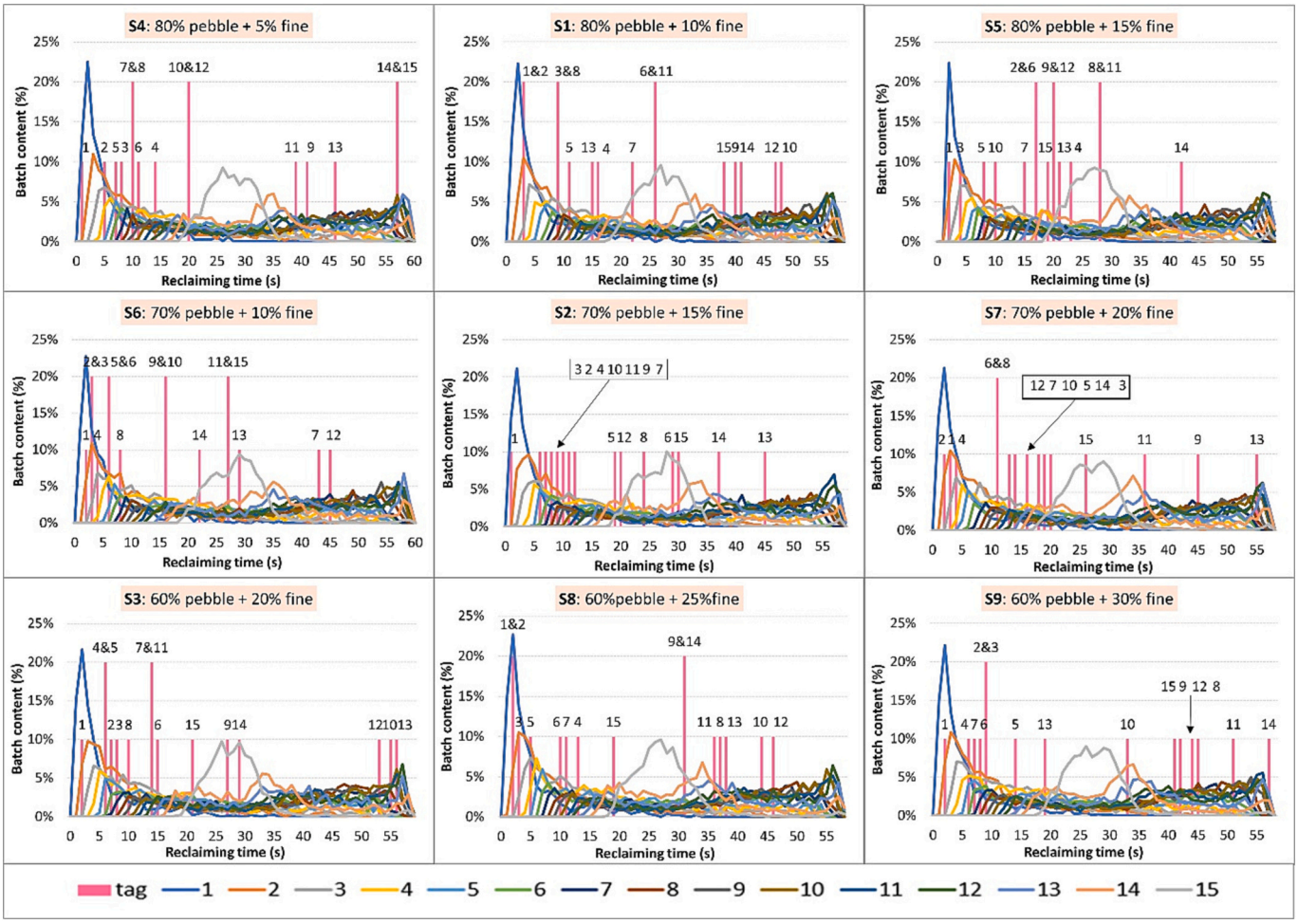

Fig. 11. Sensitivity analysis of ore tracking through COS with respect to ore size distribution (Scenarios 4 to 9).

approximation of a 37° angle of repose [26]. In this paper, clusters of five spheres were created to represent ores and repose angle test has been conducted for baseline scenario, where the angle of reposes settles around 37°. In this study copper ore particles were modelled as a cluster of five spheres consisting of uniform material. This is an approximation of bulk material which is typically heterogenous in size, shape and material; the approximation was made because of the limitations of the EDEM software and computational requirements. In the EDEM software, irregular particles can be created by clustered spheres. As the bulk material is heterogeneous and not perfectly spherical, the Young's modulus and Poisson's ratio of the bulk material cannot be directly applied within the simulation and it requires the use of representative equivalent values for these variables [25]. An approximate size distribution of distinct fine, pebble and coarse particles was used as it was not feasible to replicate the full range of particle sizes and shapes of a typical copper ore due to computational limitations [39]. A diameter of 130 mm was selected for the pebble ore particles to represent the P80 size of a typical primary gyratory crusher which processes the ore prior to the COS. The material properties of the wall are the same as the ore as the wall represents the boundary of the flow region within the stockpile.

The interactions between the modelled copper ore and other simulated materials are summarized in Table 3. The ore-tag, ore-belt, ore-steel, and tag-steel rolling friction coefficients are assumed to be 0.01. To determine the effects of coefficient of rolling friction between ore and tag, ore and belt on the blending behaviour of the COS system, a parameter sensitivity study is designed.

2.4. Sensitivity analysis

The input variables used in the simulation have a large impact on the modelled results as they are used to calculate the forces and torques within the contact model, which determine the position and orientation of particles within the model. Sensitivity analysis is a mathematical technique that can be performed to systemically investigate the effect of a range of input variables on the simulation results. To investigate the sensitivity of the DEM COS model on the simulation variables used, a series of DEM simulation scenarios were conducted to examine which variables affect the simulation results and to what extent. Table 4 and Fig. 5 presents all the variables which were investigated to determine which are crucial for accurately modelling the ore flow through the COS for ore tracking and how changes in the variables affect the ore flow. In total, 28 cases have been simulated to investigate a range of variables including the particle size distribution, particle size range, RFID tag size, stockpile wall friction, the trajectory of charging particles and the charging methods and contact model.

The ranges of the seven variables summarized in Table 4 were chosen to represent typical conditions at a copper mine. Scenarios 1 to 9 investigate the influence of the ore particle size distribution. For scenarios 1 to 3, the percentage of pebbles decreases from 80% to 60% with the same proportion of fine and coarse particles. This set of simulation scenarios provides a means of investigating how the proportion of pebble particles affects particle flow through the COS and the association between ore batches and RFID tags. In Scenarios 4 to 9, the

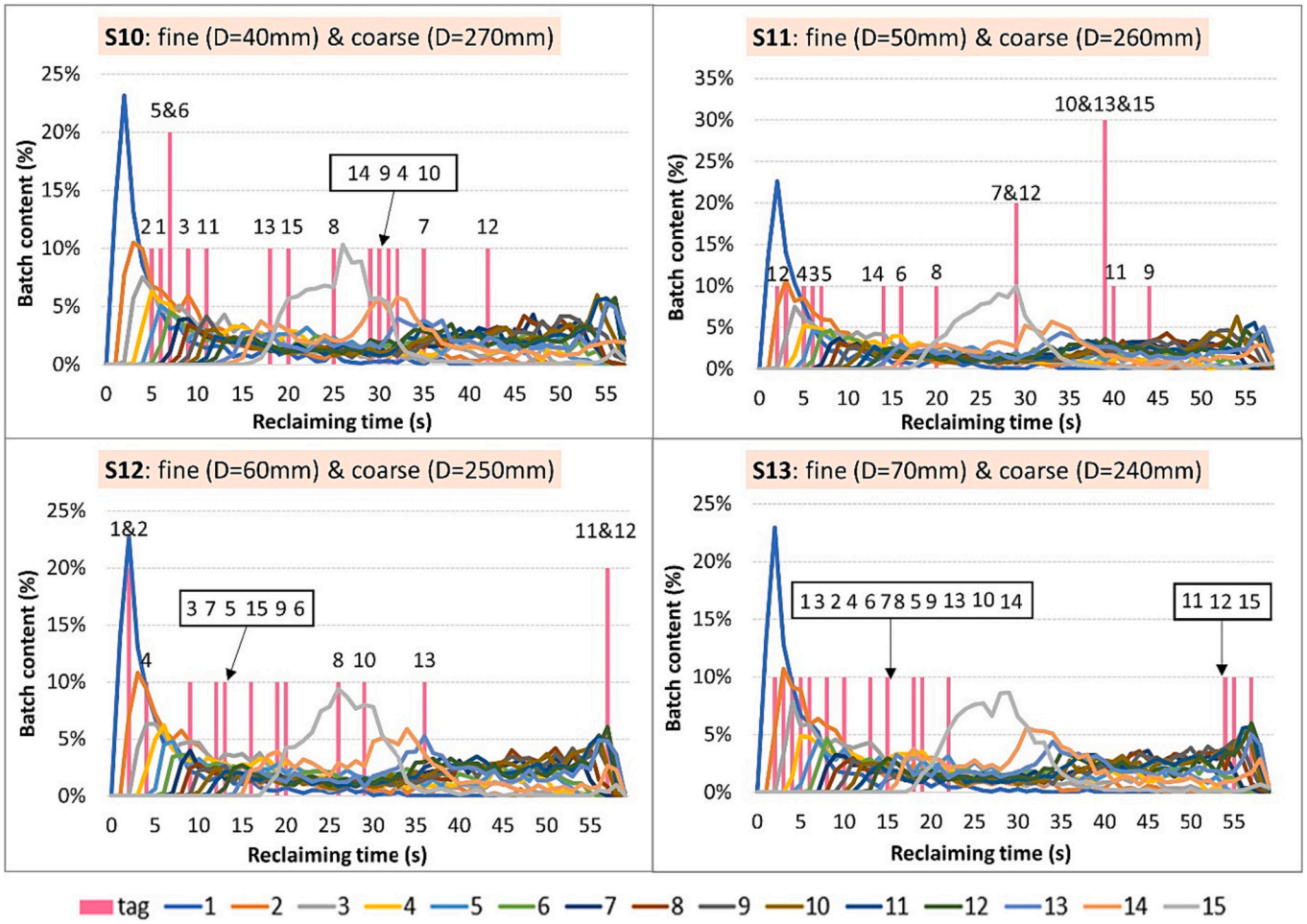

Fig. 12. Sensitivity analysis of ore tracking through COS with respect to ore size range.

percentage of fine particles increases from 5% to 15%, 10% to 20%, and 25% to 30% while the proportion of pebble particles remains constant at 80%, 70%, and 60% respectively. This set of simulation scenarios investigates how a large proportion of fine particles affects particle flow through the COS and the association between ore batches and RFID tags.

Scenarios 10 to 13 investigate the influence of the ore size range. It is important to study this as the ore size range varies in real time depending on the mined material. These simulation scenarios examine how the material size range can affect the discharge of the materials and the association between ore batches and RFID tags.

Scenarios 14 to 17 study the effect of the RFID tag size. The simulated RFID tag sizes are smaller than most of the particles in the model which can affect the transport of the tags relative to the ore particles. These scenarios investigate whether the tag size affects the link between ore batches and their associated tags.

Scenarios 18 to 20 investigate the influence of wall friction. The modelled conical boundary approximates the live component of a stockpile implemented to reduce computational requirements. To determine the sensitivity of the simulation to this approximation, a range of different wall friction values were simulated.

Scenarios 21 to 23 study the effect of particle trajectory. Varying the conveyor belt velocity from 2 to 5 m/s changes the trajectory of the charging ore flow and hence the fill location. A range of belt velocities were examined to evaluate the effect of the fill position and impact velocity and angle on the resulting stockpile shape, the discharging of material and the association between ore batches and RFID tags.

Scenarios 24 to 26 investigate the effect of when stockpile reclamation commences within the simulation. Cases in which reclamation starts when filling is between 60% to 100% completion are simulated. These simulations provide information on how the combination of filling and reclamation methods affect the discharge of the material and the association of tags with their respective batches.

Scenarios 27 and 28 consider the use of the linear spring dashpot and Hertz-Mindlin with JKR models to examine the influence of the contact model. The linear spring dashpot model is commonly used to model the interaction between particles. The Hertz-Mindlin with the JKR model takes the material moisture content into account, allowing the modelling of wet and sticky particles [42]. A surface energy of 10 J/m^2, static friction of 0.3 and rolling friction of 0.06 were found to be the appropriate JKR model coefficients via repose angle testing as detailed by Roessler and Katterfeld [43].

Scenarios 29 to 34 investigate the effect of assumed values used in the simulation such as the ore-tag and ore-belt rolling friction coefficients. As the steel has limited contact with the ore and tag during the simulation, the effects of the assumed ore-steel and tag-steel rolling friction coefficients are not investigated.

3. Results and discussion

The typical ore flow observed over the feeding and reclamation processes is shown in Fig. 6. It was found that multiple ore batches, shown in different colours, are mixed during the ore reclamation process.

Fig. 7 shows the percentage of each ore batch content reclaimed

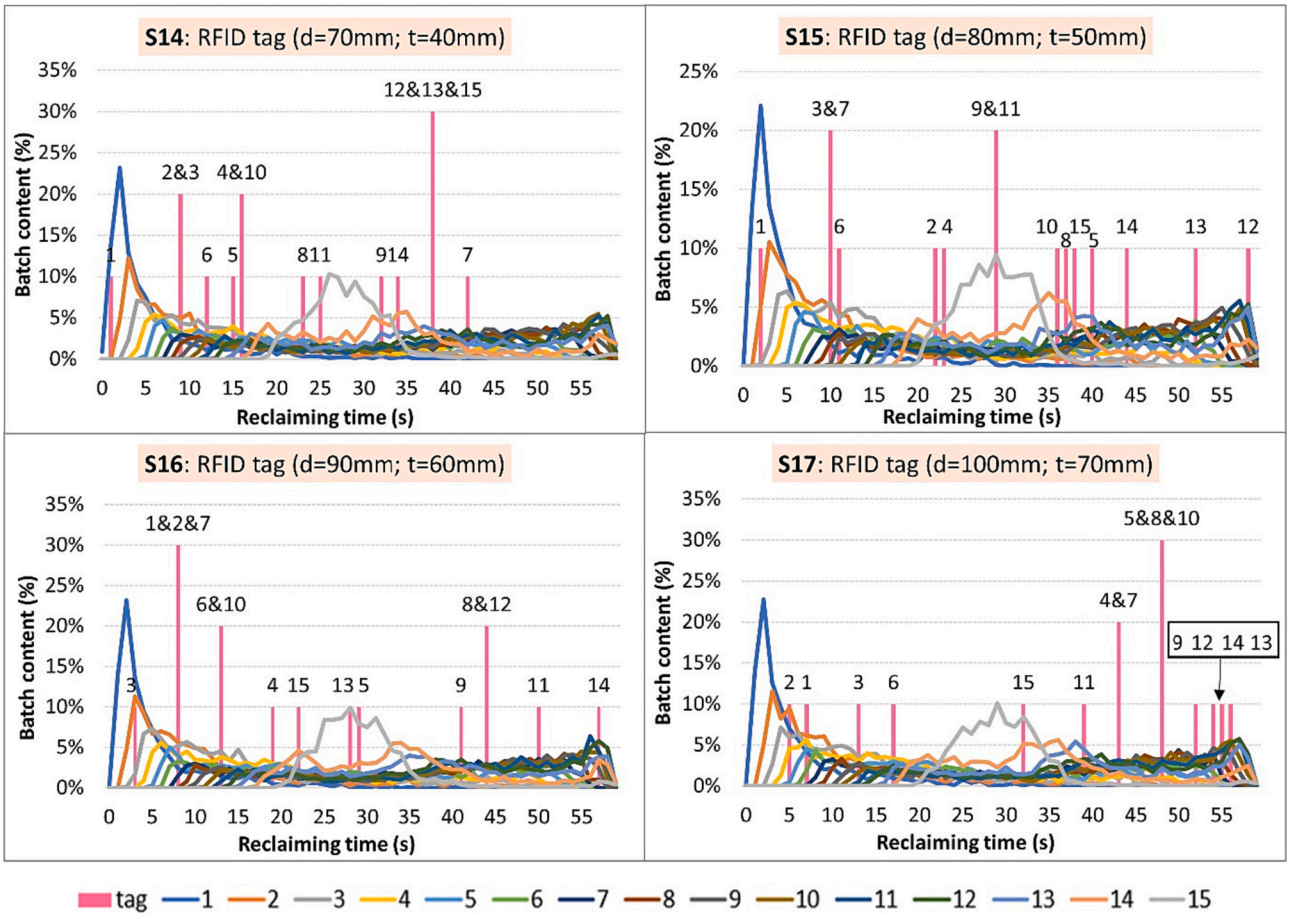

Fig. 13. Sensitivity analysis of ore tracking through COS with respect to RFID tag size.

during every second of the stockpile discharging process as well as the time that each RFID tag is scanned by the virtual reader for the baseline scenario. Due to the randomness inherent in particle motion, the time and order in which the RFID tags are read can vary significantly. As such, repeat tests of the baseline scenario (Fig. 8) have been conducted to test the range of potential results.

In EDEM, the particle generation mechanism is configured as an unlimited number model in which particles are randomly generated on a plane. During the initial particle generation, the positions of the particles are determined using a random number generator. The random number generator is reset each time that a simulation is started so as to ensure different particle distributions in each run. To conduct a repeatability test, four identical simulations with the same parameter settings were performed. This ensures that the simulation parameters, such as particle properties, boundary conditions, and forces, were the same for each run. By running multiple simulations with identical parameters, the consistency and reproducibility of the results can be assessed. All the batches in each repeat test showed the same general trend, which confirms that the test is repeatable and that the results can be used with confidence.

The results show that most RFID tags were reclaimed prior to their associated ore batch and that the tags were not reclaimed in the order that they were introduced. The time interval between tags varied between 1 and 9 s, with some tags closely clustered together and some tags well separated from the next. The tags being read before their respective batch indicates that the small RFID smart tags passed through the stockpile faster than the larger ore particles. This result is consistent with Jansen's findings that smaller stockpile retention tracers were reclaimed first while the coarsest were reclaimed last due to a general trend of longer average retention times for larger size fractions [44]. As RFID tags are generally reclaimed early and out of order, they are poorly representative of their original ore batches and quantitative information correlated to the ore batch is lost. Particle and tag segregation depends on the material interactions and may vary for different ore types and material characteristics; it is also affected by the calibration of the relevant parameters within the simulation. In this case, increased numbers of RFID tags would be required for each batch in order to ensure the association of the tags with their respective ore batches.

As well as providing information on the association of tags with their ore batches, Fig. 7 also provides information on how each batch was reclaimed. This information is vital for understanding how ore and RFID tags move and interact within the stockpile. The reclamation of the first ore batch reaches a peak of about 23% at a time of 2 s. The second, third and fourth ore batches reach peaks of 10%, 7% and 5% at 3, 4 and 5 s respectively. The total stockpile discharging and apron feeder reclaiming process occurs over approximately 60 s and, except for the first 10 s and the last 5 s, ore batches (excluding batch 15) are reasonably evenly blended with about 2–4% of each ore batch being reclaimed each second. The overall retention time of batch 15, the last ore batch represented by the light grey line in Fig. 7, is shorter than most of the other batches. These results compare well to the findings of Parker [45] who found that ore batches closer to the centre of the stockpile, located directly above the discharge point, tend to travel faster through the stockpile than batches further down the outer slopes of the stockpile. The cross-section of the discharging process presented in Fig. 9 shows that a steep inner discharge cone forms at the top of the stockpile which

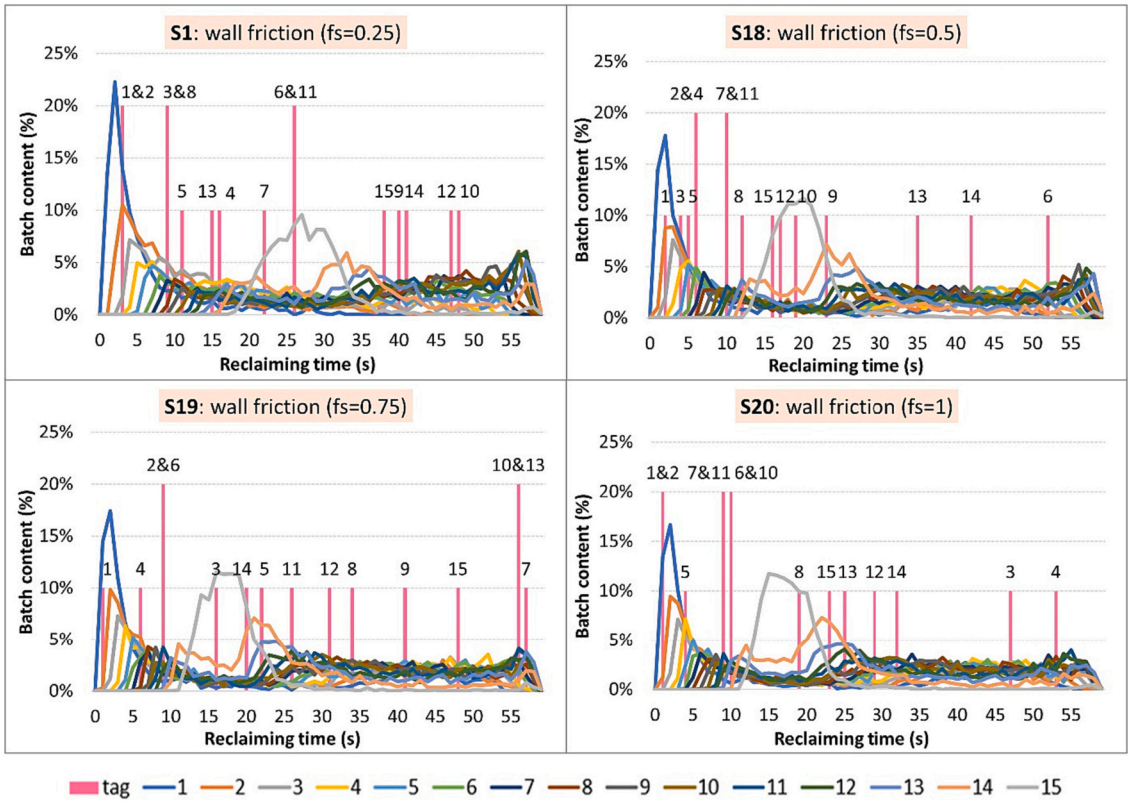

Fig. 14. Sensitivity analysis of ore tracking through COS with respect to wall friction.

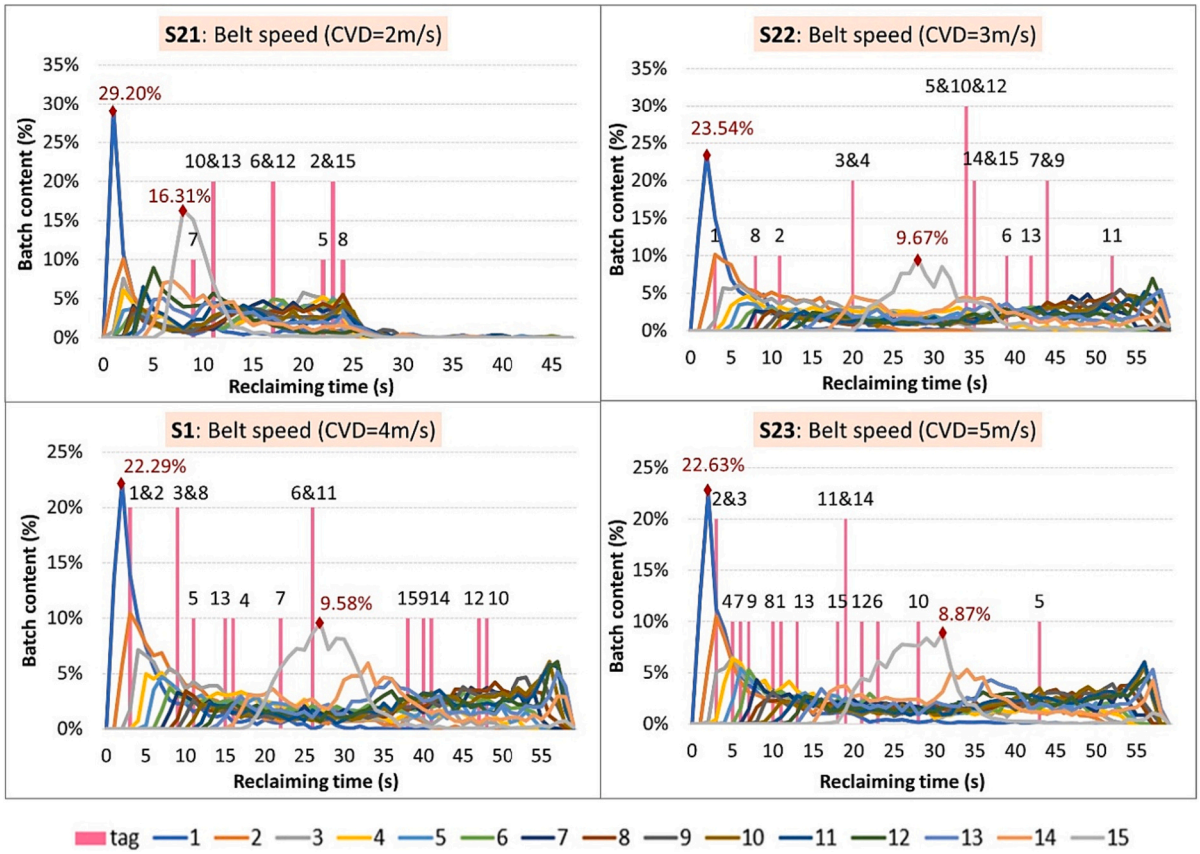

Fig. 15. Sensitivity analysis of ore tracking through COS with respect to stockpile feed belt speed.

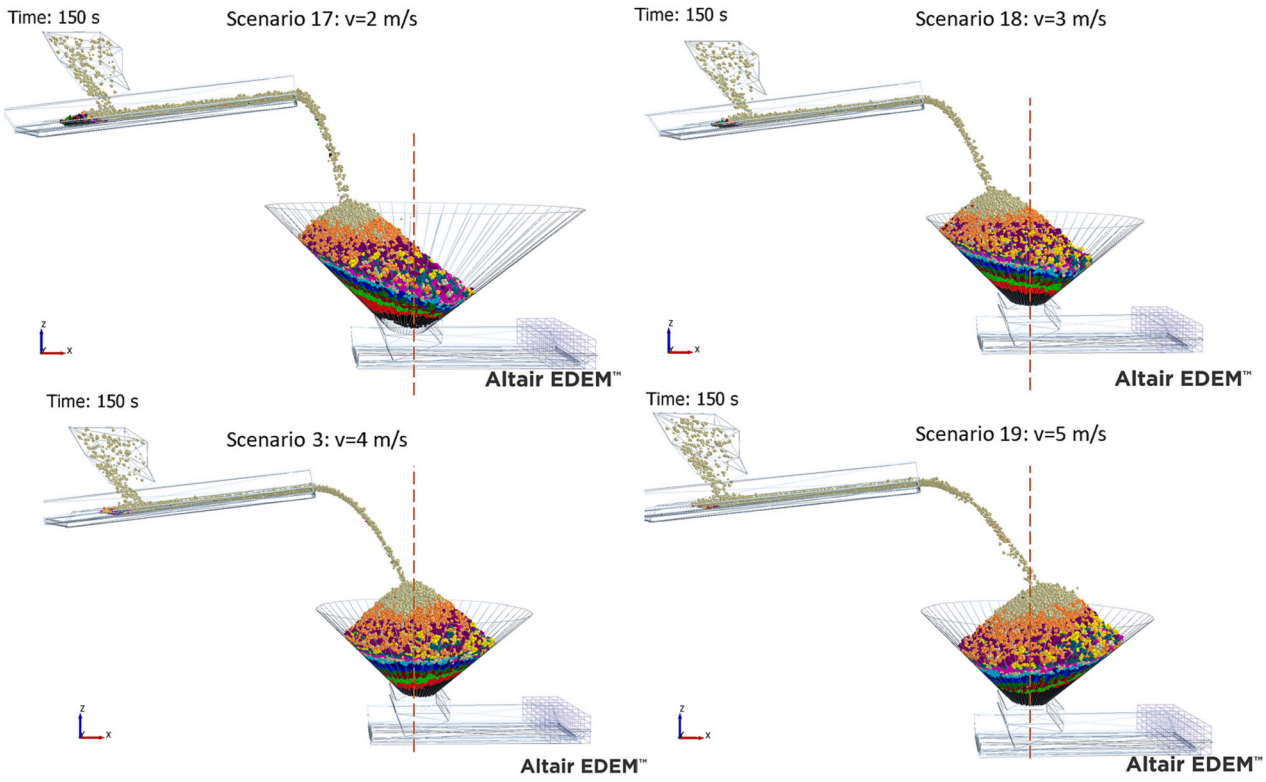

Fig. 16. Stockpile shape for different feed belt speeds.

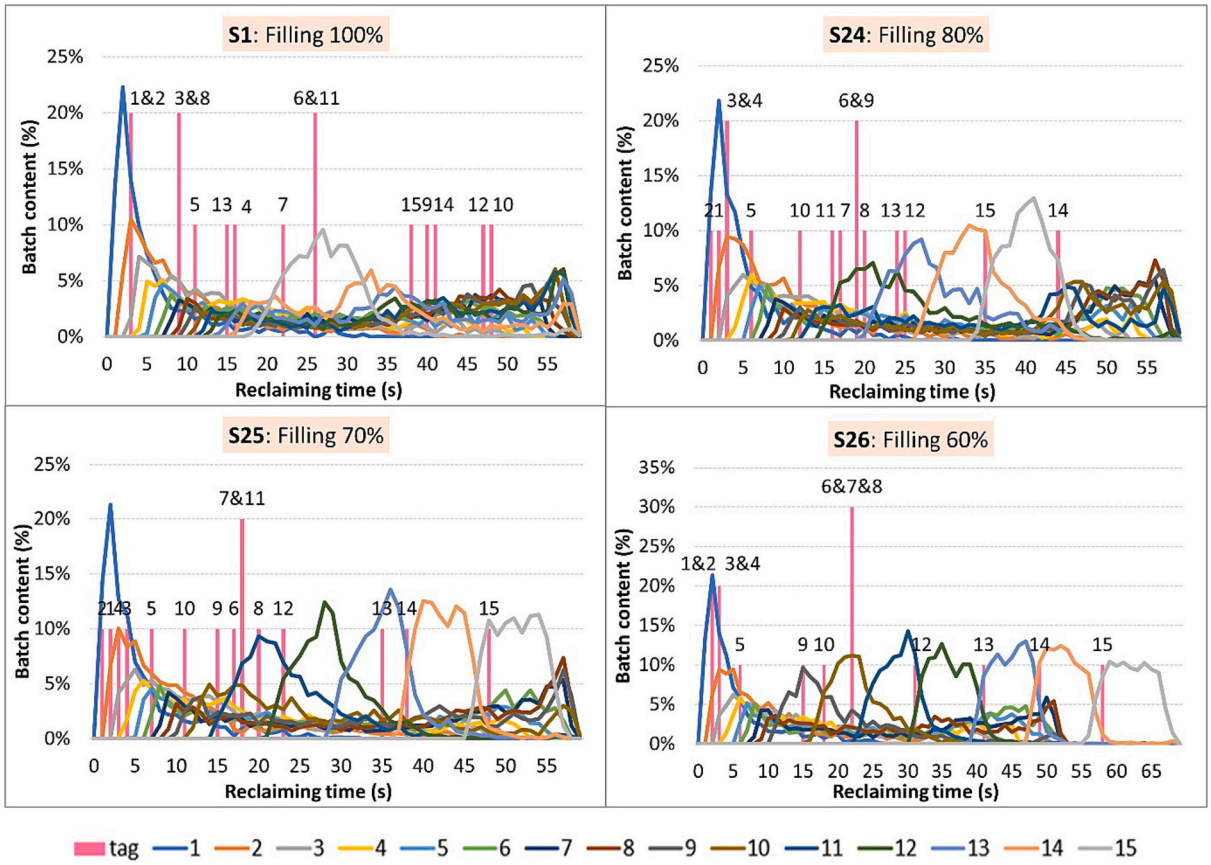

Fig. 17. Sensitivity analysis of ore tracking through COS with respect to stockpile storage percentage.

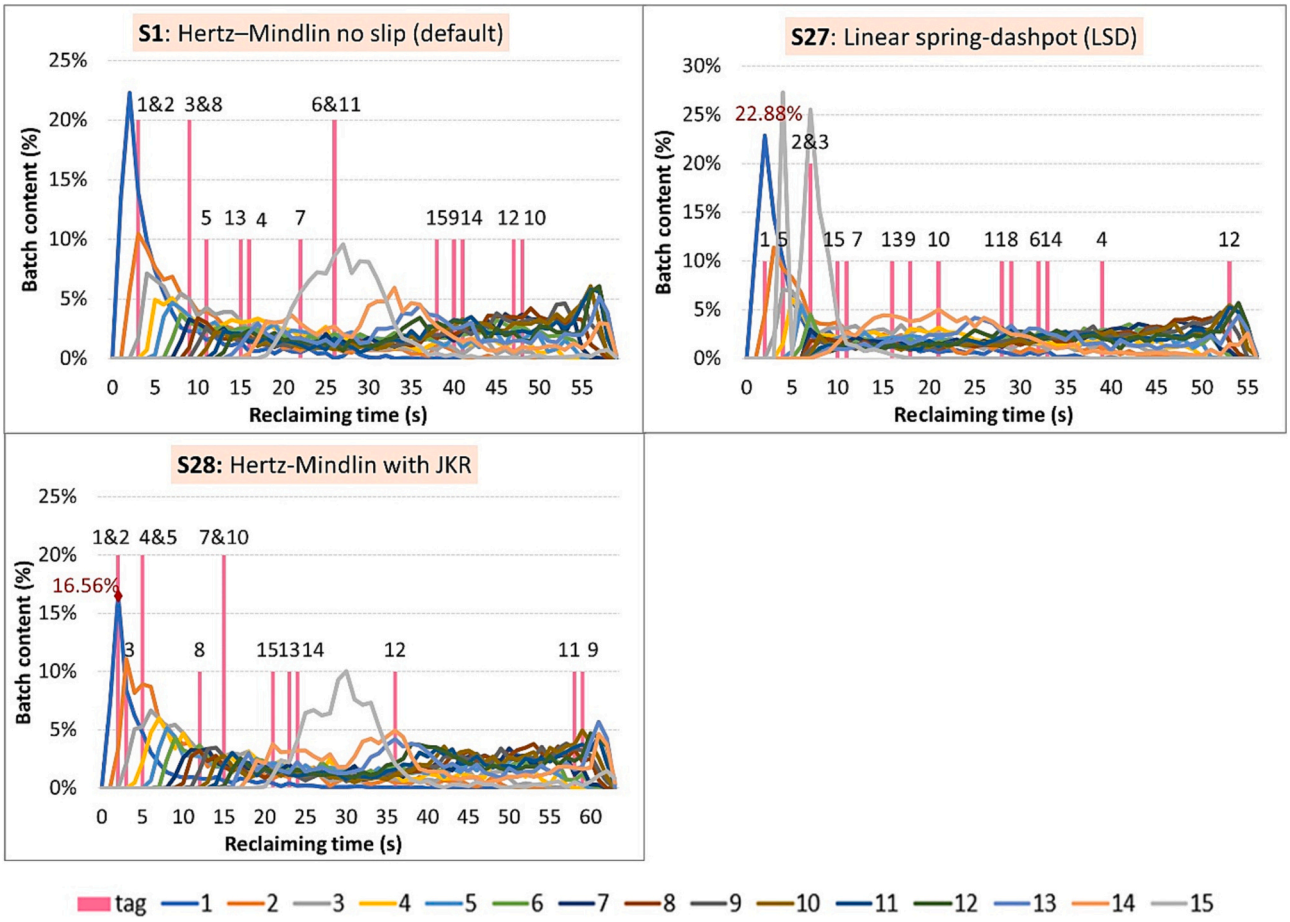

Fig. 18. Sensitivity analysis of ore tracking through COS with respect to contact model.

eventually widens outwards to produce a discharge cone with a lateral shape. This result is consistent with Parker's findings that ores closer to the stockpile withdrawal wall remain motionless and are less affected by other ore flows following the opening of the discharge point [45]. The formation of this discharge cone is significant because it influences the flow of ore particles during the extraction process. As the discharge point is opened, ore particles start to move and flow downwards. Parker's findings suggest that the behaviour of ore particles in the discharge cone is not uniform throughout the cone's shape. Closer to the withdrawal wall of the stockpile, where the discharge point is located, the ore particles tend to remain motionless or experience minimal movement. This is because these particles are shielded by other particles around them, forming a more stable region. They are less affected by the flows of ore occurring in other parts of the discharge cone. In contrast, the ore particles located further away from the withdrawal wall experience greater interaction with other flowing particles. These particles are more influenced by the bulk flow and movement of the ore as it cascades down the discharge cone. This results in a wider lateral shape of the discharge cone, as the particles closer to the withdrawal wall have limited lateral movement.

The effect of a change in the particle size distribution on the ore batch and tag discharge is shown in Figs. 10 and 11. It was found that as the proportion of the ore consisting of fine and coarse particles is varied, there was only a minimal effect on the batch mixing and discharging. This indicates that the COS is not sensitive to the change in the coarse and fine balance.

The effect of the ore particle size range on ore and tag reclamation is shown in Fig. 12. It was found that the ore size range has only a very small effect on the batch blending behaviour as it passes through the stockpile. This indicates that, as for the particle size distribution, the COS simulation is not sensitive to changes in the particle size range.

The effect of the tag size on the reclamation of the tags and their corresponding batches is shown in Fig. 13. As expected, given the small number of tags relative to particles there was no impact on the ore batch mixing within the COS. There was no discernible effect of the tag size on the association between ore batches and their RFID tag. However, smaller effects would be hard to identify due to the uncertainty of the tag distribution. A small effect of the tag size is reasonable as the size range considered, which is representative of typical RFID tags, is smaller than most of the simulated ore particles.

Fig. 14 shows the effect of the simulated wall friction on the transport of the ore batches and tags through the COS. It was found that as the wall friction increases the last ore batch is reclaimed earlier. It was also observed that the initial peaks of the first batch were reduced while the peaks of the last three batches increased with increasing friction. These results indicate that the ore close to the wall moves more slowly with increased friction resulting in the ore close to the centre of the stockpile flowing faster and being reclaimed earlier.

The effect of the feed belt velocity on ore batch blending and the distribution of the RFID tag readings is shown in Fig. 15. It was observed that reclamation of the last ore batch occurred later as the conveyor belt speed increased. Fig. 16 shows the effect of the feed belt speed on the distribution of the ore filling the stockpile. The fill point and resulting peak of the stockpile is further from the belt as the velocity is increased. As the tip of the stockpile moves further away from the centreline of the stockpile, for low feed velocities, the total stockpile charging and apron

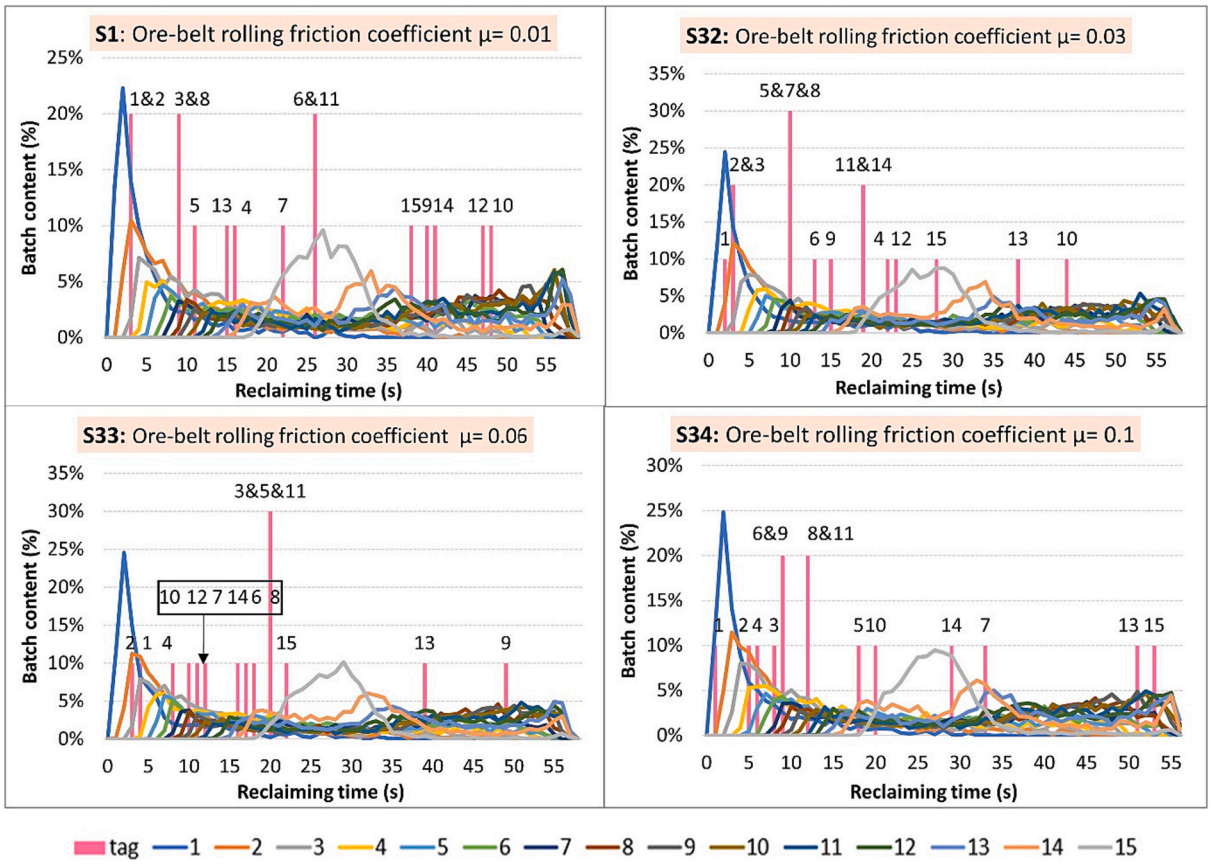

Fig. 19. Sensitivity analysis of ore tracking through COS with respect to rolling friction coefficient between ore and tag.

feeder reclaiming time is reduced and the peak reclamation for the first and last batch is increased to 29% and 16% respectively.

Fig. 17 shows the effect of the time at which the filling process reclamation is begun on the ore batch blending and tag association. It was found that when reclamation was begun earlier in the simulation, a majority of the COS stockpile was reclaimed prior to the later batches being fed into the COS. This resulted in a reduction in the segregation of the later ore batches, resulting in a good association between the batches and their respective ore tags.

The effect of the EDEM contact model used on the ore batch blending and tag association is shown in Fig. 18. The variety of particle sizes and modelled ore batches combined with the presence of the tags results in a wide range of potential particle interaction pairs. This, together with the large number of particles modelled, causes the Hertz-Mindlin models to be computed faster than the linear spring dashpot model. For the linear spring dashpot contact model, the last ore batch shown in light grey in Fig. 18 was extracted earlier than most of the other ore batches. The extraction of this batch occurred at a later point in the Hertz-Mindlin models. Evaluation of the discharge showed that, for the linear spring dashpot model, an extremely steep discharge cone developed causing the rapid discharge of the final batch which is not representative of the discharge of a real stockpile. This shows that the Hertz-Mindlin models were better able to represent realistic stockpile discharges as well as being less computationally expensive. The Hertz-Mindlin with JKR contact model simulates the effect of the moisture between particles. It was found that, apart from reducing the initial extraction of the first batch from 22% to 17%, the JKR moisture model has only a small effect on the batch blending behaviour as it passes through the stockpile compared to the default Hertz-Mindlin model.

Figs. 19 and 20 show the effect of the ore-tag and ore-belt rolling friction coefficients used in the simulation on the blending of ore batches within the COS. The effects of the assumed coefficients are explored with the variables from the references. As the ore-tag rolling friction coefficient increases, there is no discernible impact on the ore batch mixing within the COS. This is likely due to the small number of tags relative to particles within the simulation. There was only a minimal effect on the batch mixing and discharging as the ore-belt rolling friction coefficient increases. This indicates that the COS is not sensitive to the change in the coefficient of rolling friction between ore and the belt.

The results of the sensitivity study are summarized in Table 5. The DEM COS model results show that variables such as ore size distribution, ore size range, RFID tag size, rolling friction coefficient between ore and tag do not have a significant impact on the transport of ore through a COS while variables such as wall resistance, the trajectory of charging particles (stockpile feed belt speed), stockpile storage percentage and EDEM contact model do have a significant impact.

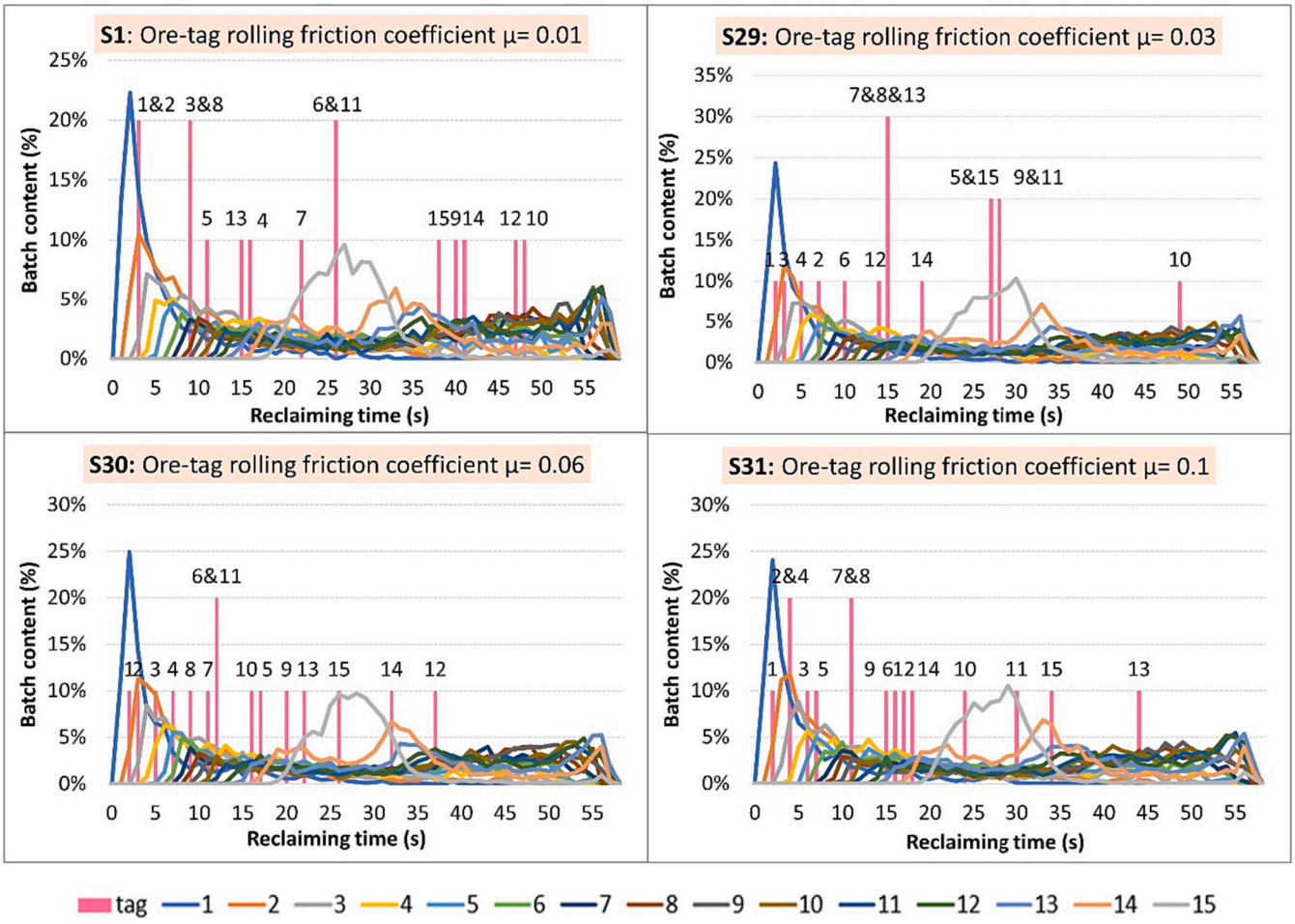

Fig. 20. Sensitivity analysis of ore tracking through COS with respect to rolling friction coefficient between ore and belt.

Table 5
Summary of sensitivity study results.

Categories	EDEM parameters	Scenarios	Sensitivity
Bulk material size distribution	ore size distribution (pebble percentages)	1–3	Low
	ore size distribution (fine percentages)	4–9	Low
Bulk material size range	ore size range	10–13	Low
RFID tag size	RFID tag size	14–17	Low
Wall resistance	coefficient of static friction	18–20	High
Trajectory of charging particles	stockpile feed belt speed	21–23	High
Stockpile storage percentage	stockpile storage percentage	24–26	High
Contact model	contact model	27–28	High
Rolling friction coefficient	rolling friction coefficient ore -tag	29–31	Low
	rolling friction coefficient ore -belt	32–34	Low

4. Conclusions

The DEM modelling of the transport of ore and RFID tags through a coarse ore stockpile and apron feeder presented in this paper provides for the first time information on the association of tags with their ore batches through a 3D COS. Additionally, a sensitivity analysis of the DEM input variables was conducted to provide information on which variables affect the transport through the COS. This sensitivity study suggests that DEM may be an excellent tool to investigate the correlation between RFID tags and discharging materials under different scenarios, which is difficult to obtain experimentally.

The proposed modelling framework fills the gaps in previous models by using a three-dimensional modelling approach. The results of the sensitivity study provided critical information on the blending behaviour of tags and ore batches within the stockpile, showing that:

(1) Ore batches closer to the centre of the stockpile, directly above the discharge point, flow faster through the stockpile than the ore batches close to the wall. In particular, when the wall friction increases, ore batches closer to the centre of the stockpile (last batch) travelled faster through the COS.
(2) The overall performance of RFID-based ore tracking through the stockpile is poor. Most RFID tags were reclaimed prior to their associated ore batch. This indicates that the tags, being smaller than even the fine ore particles, pass through the stockpile faster than the ore. It was also observed that the interval between tags varied from 1 to 9 s.
(3) The RFID tags scanned by the virtual reader were out of order. This unexpected phenomenon may be due to flow-induced segregation within the apron feeder. Segregation of materials in the ore flow region could increase the uncertainty of the association between ore batches and RFID tags. If such segregation occurs, the variability of particle transport within the COS system will increase. The number of RFID tags used for each batch to ensure association between the tags and ore batches needs to be determined.

(4) The particle size distribution, particle size range, RFID tag size, and ore-tag and ore-belt rolling friction coefficients were found to have limited impact on the stockpile batch blending behaviour. The percentages of ore from each batch during the discharging process have similar trends for all evaluated values of these variables.

The DEM COS model demonstrated high sensitivity to changes in wall friction, stockpile storage percentage, stockpile feed belt speed and contact model, while it showed low sensitivity to variables such as the ore size distribution, ore size range, RFID tag size and ore-tag and ore-belt rolling friction coefficients. Simulations of the COS including a sensitivity analysis can be useful to model ore transport through a COS and to provide an improved understanding of batch and tag transport to help track ore through a COS.

CRediT authorship contribution statement

Juan Chen: Conceptualization, Software, Methodology, Data curation, Formal analysis, Writing- Original draft preparation, Visualization. **Tien-Fu Lu**: Resources, Supervision, Writing - Review & Editing. **Dylan Peukert**: Supervision, Writing - Review & Editing. **Peter Dowd**: Supervision, Resources, Supervision, Writing - Review & Editing.

Declaration of Competing Interest

The authors declare the following financial interests/personal relationships which may be considered as potential competing interests:

Juan Chen reports financial support was provided by Australian Research Council Integrated Operations for Complex Resources Industrial Transformation Training Centre.

Data availability

Data will be made available on request.

Acknowledgments

The authors thank Altair EDEM Ltd. for their support in providing the EDEM® 2021.1 simulation software to complete the work presented here.

The research of Juan Chen was supported by the Australian Research Council Integrated Operations for Complex Resources Industrial Transformation Training Centre (project number IC190100017) and funded by Universities, Industry, and the Australian Government.

References

[1] L. Bandyopadhyay, S. Chaulya, P. Mishra, Wireless information and safety system for mines, in: Wireless Communication in Underground Mines, Springer, 2010, pp. 175–262.
[2] X. Zhang, Smart Sensor and Tracking System for Underground Mining, University of Saskatchewan, 2016.
[3] M.K.N. Mahmad, M.R.R. MAZ, N. Baharun, Applications of radio frequency identification (RFID) in mining industries, in: IOP Conference Series: Materials Science and Engineering, IOP Publishing, 2016.
[4] S. Fiscor, Vale Inco tracks ore with RFID tags, Eng. Min. J. 208 (10) (2007) 52.
[5] B. Kvarnström, P. Oghazi, Methods for traceability in continuous processes–experience from an iron ore refinement process, Miner. Eng. 21 (10) (2008) 720–730.
[6] D. La Rosa, et al., The Use of Radio Frequency ID Tags to Track Ore in Mining Operations, 2007.
[7] W. Kawalec, et al., Project DISIRE (H2020)–an idea of annotating of ore with sensors in KGHM Polska Miedz SA underground copper ore mines, in: E3S Web of Conferences, EDP Sciences, 2016.
[8] S. Xu, et al., Measuring bulk material flow—incorporating RFID and point cloud data processing, Measurement 200 (2022), 111598.
[9] B. Bergquist, Traceability in iron ore processing and transports, Miner. Eng. 30 (2012) 44–51.
[10] W.M. Jansen, Strategic Approach to Mine-Mill Reconciliation, 2008.
[11] P. Bardzinski, et al., Simulation of random tagged ore fow through the bunker in a belt convering system, Int. J. Simulat. Modell. 17 (4) (2018) 597–608.
[12] X. Pan, Online Smart Sensor to Measure Stockpiles Used in Mineral Processing, 2015.
[13] Y. Yu, et al., DEM and experimental studies on pellet segregation in stockpile build-up, Ironmak. Steelmak. 45 (3) (2018) 264–271.
[14] A. Yu, et al., Stockpiling behaviour as observed in a model experiment, in: 5th International Conference on Bulk Materials Storage, Handling and Transportation: Proceedings: Proceedings, Institution of Engineers, Australia Barton, ACT, 1995.
[15] Z. Ye, et al., A laboratory-scale characterisation test for quantifying the size segregation of stockpiles, Miner. Eng. 188 (2022), 107830.
[16] B. Kvarnström, S. Nordqvist, Modelling process flows in continuous processes with radio frequency identification technique, in: International Conference on Process Development in Iron and Steelmaking: 08/06/2008-11/06/2008, MEFOS, 2008.
[17] B. Kvarnström, E. Vanhatalo, Using RFID to improve traceability in process industry: experiments in a distribution chain for iron ore pellets, J. Manuf. Technol. Manag. 21 (1) (2009) 139–154.
[18] B. Bergquist, E. Vanhatalo, In-situ measurement in the iron ore pellet distribution chain using active RFID technology, Powder Technol. 361 (2020) 791–802.
[19] P.A. Cundall, A computer model for simulating progressive, large-scale movement in blocky rock system, in: Proceedings of the International Symposium on Rock Mechanics, 1971, p. 1971.
[20] P.A. Cundall, O.D. Strack, A discrete numerical model for granular assemblies, geotechnique 29 (1) (1979) 47–65.
[21] Y. Yu, H. Saxén, Experimental and DEM study of segregation of ternary size particles in a blast furnace top bunker model, Chem. Eng. Sci. 65 (18) (2010) 5237–5250.
[22] D. Hastie, Belt Conveyer Transfers: Quantifying and Modelling Mechanisms of Particle Flow, 2010.
[23] G. Delaney, et al., Predicting breakage and the evolution of rock size and shape distributions in ag and SAG mills using DEM, Miner. Eng. 50 (2013) 132–139.
[24] G.K. Barrios, et al., DEM simulation of laboratory-scale jaw crushing of a gold-bearing ore using a particle replacement model, Minerals 10 (8) (2020) 717.
[25] D. Ilic, A. Lavrinec, O. Orozovic, Simulation and analysis of blending in a conveyor transfer system, Miner. Eng. 157 (2020), 106575.
[26] E. Dolman, Modelling of Material Flow and Size Distribution of Ore in a Stockpile at Tara Mines, Ireland, 2012.
[27] R. Gómez, et al., Segregation modeling in stockpile using discrete element method, Appl. Sci. 12 (23) (2022) 12449.
[28] D. Zhang, Z. Zhou, D. Pinson, DEM simulation of particle stratification and segregation in stockpile formation, in: EPJ Web of Conferences, EDP Sciences, 2017.
[29] S. Zhao, et al., Automatic quality estimation in blending using a 3D stockpile management model, Adv. Eng. Inform. 29 (3) (2015) 680–695.
[30] Z. Zhou, et al., Discrete particle simulation of gas–solid flow in a blast furnace, Comput. Chem. Eng. 32 (8) (2008) 1760–1772.
[31] A. Di Renzo, F.P. Di Maio, Comparison of contact-force models for the simulation of collisions in DEM-based granular flow codes, Chem. Eng. Sci. 59 (3) (2004) 525–541.
[32] Y. Tsuji, T. Tanaka, T. Ishida, Lagrangian numerical simulation of plug flow of cohesionless particles in a horizontal pipe, Powder Technol. 71 (3) (1992) 239–250.
[33] J. Zhang, et al., Application of the discrete approach to the simulation of size segregation in granular chute flow, Ind. Eng. Chem. Res. 43 (18) (2004) 5521–5528.
[34] H. Hertz, Über die Berührung fester elastischer Körper, Journal für die reine und angewandte Mathematik 92 (156–171) (1882) 22.
[35] H.A. Navarro, M.P.D.S. Braun, Linear and nonlinear Hertzian contact models for materials in multibody dynamics [Internet], Anais (2013); Available from: http://www.abcm.org.br/anais/cobem/2013/PDF/68.pdf.
[36] Y. Zhou, et al., Rolling friction in the dynamic simulation of sandpile formation, Phys. A: Stat. Mech. Appl. 269 (2–4) (1999) 536–553.
[37] J. Horabik, M. Molenda, Parameters and contact models for DEM simulations of agricultural granular materials: a review, Biosyst. Eng. 147 (2016) 206–225.
[38] R.D. Mindlin, Compliance of Elastic Bodies in Contact, 1949.
[39] A.P. Grima, P.W. Wypych, Investigation into calibration of discrete element model parameters for scale-up and validation of particle–structure interactions under impact conditions, Powder Technol. 212 (1) (2011) 198–209.
[40] M. Wortley, E. Nozawa, K. Riihioja, Metso SmartTag–the next generation and beyond, in: 35th APCOM Symposium, 2011.
[41] D. Schulze, Silo Design for Flow, Powders and Bulk Solids: Behavior, Characterization, Storage and Flow, Springer, Berlin, Germany, 2008.
[42] S. Karkala, et al., Calibration of discrete-element-method parameters for cohesive materials using dynamic-yield-strength and shear-cell experiments, Processes 7 (5) (2019) 278.
[43] T. Roessler, A. Katterfeld, DEM parameter calibration of cohesive bulk materials using a simple angle of repose test, Particuology 45 (2019) 105–115.
[44] W. Jansen, et al., Tracer-based mine-mill ore tracking via process hold-ups at Northparkes mine, in: Tenth Mill Operators' Conference, Adelaide, SA, 2009.
[45] B.M. Parker, The Simulation and Analysis of Particle Flow through an Aggregate Stockpile, Virginia Tech, 2009.